MNRAS **000**, 1–21 (2020) Preprint 23 October 2020 Compiled using MNRAS LATEX style file v3.0

The GALAH Survey and Symbiotic Stars. I. Discovery and follow-up of 33 candidate accreting-only systems

Ulisse Munari,[1]★ G. Traven,[2] N. Masetti,[3,4] P. Valisa,[5] F.-J. Hambsch,[5] A. Frigo,[5] and the GALAH Collaboration

[1] *INAF Astronomical Observatory of Padova, 36012 Asiago (VI), Italy*
[2] *Lund Observatory, Department of Astronomy and Theoretical Physics, Box 43, SE-221 00 Lund, Sweden*
[3] *INAF Osservatorio di Astrofisica e Scienza dello Spazio, via Gobetti 93/3, 40129 Bologna, Italy*
[4] *Departamento de Ciencias Físicas, Universidad Andrés Bello, Fernández Concha 700, Las Condes, Santiago, Chile*
[5] *ANS Collaboration, c/o Astronomical Observatory, 36012 Asiago (VI), Italy*

Accepted XXX. Received YYY; in original form ZZZ

ABSTRACT

The GALAH spectroscopic survey of the Southern Hemisphere with the 400-fibre positioner at the AAO 4m telescope in Australia has recorded high resolution spectra ($R_P \sim 28\,000$) for 600 255 stars included in its Data Release 3. We have identified 15824 M-type giants among them (luminosity class III and higher). About 223 of them were found to show an emission in Hα with a peak in excess of 0.5 above the adjacent continuum level. Probable radial pulsators among them were identified based on lightcurves built from multi-year ASAS-SN sky-patrol photometry, and eliminated. Together with a vast array of follow-up confirmatory observations (X–ray/UV observations with the *Swift* satellite, search for optical flickering, presence of a near-UV upturn in ground-based photometric and spectroscopic data, radial velocity changes suggestive of orbital motion, variability of the emission line profiles) and guided from a step-by-step comparison with the properties of the prototype SU Lyn, we have identified 33 new candidates for symbiotic stars of the accreting-only variety and we encourage further observations to confirm/document their symbiotic star nature. The M giant of one of them shows a large over-abundance in ^{7}Li, possibly the result of pollution from an unrecorded nova outbursts. This is the first in a series of studies that will closely examine symbiotic stars in the GALAH survey, with following ones dedicated to investigating spectral types other than M, with a weaker emission in Hα, or reviewing the chemical/dynamical properties of symbiotic stars as a whole, including their proposed role as progenitors of type Ia supernovae.

Key words: binaries: symbiotic stars – methods: data analysis – Galaxy: stellar content

1 INTRODUCTION

Symbiotic stars (SySt) are interacting binaries where a red giant (RG) fuels a white dwarf (WD) or a neutron star (NS) companion via accretion (either through Roche-lobe overflow or wind intercept). Systems harboring NSs are a recent addition to this class of celestial objects and constitute a few percent of the known total, the vast majority containing WDs. The RG+WD symbiotic stars are broadly divided into two major groups (see the recent review by Munari 2019 for details): those *accreting-only* (AO-SySt) whose optical spectra are dominated by the RG with no or weak emission lines, and the *burning-type* (NB-SySt) displaying a strong nebular continuum and a rich emission line spectrum: they originate from the wind of the RG, which is largely ionised by the very hot and luminous WD undergoing surface nuclear burning of accreted material.

SySt are believed to spend most of their time in the accreting-only phase, quietly accumulating material on the surface of the WD. When enough has been piled up, nuclear burning ignites. If the accreted matter is electron degenerate, the burning proceeds explosively. It reaches the Fermi temperature in a matter of minutes (Starrfield et al. 2008) and ejects most (or all) of the accreted envelope at high ve-

★ E-mail: ulisse.munari@inaf.it

locity (thousands of km s^{-1}). The resulting nova outburst can repeat on time-scales as short as years/decades if the WD mass is close to the Chandrasekhar limit, as it is the case for T CrB, RS Oph, V3890 Sgr, or V407 Cyg, the last one being the first nova detected in GeV γ-rays by the Fermi satellite (Cheung et al. 2010). If the matter accreted on the WD is instead not electron-degenerate, the nuclear burning will proceed in thermal equilibrium, taking a few years to reach peak brightness (Fujimoto 1982), and requiring many decades to a few centuries to burn the accreted envelope and let the system to return to low luminosity. Some of the best examples of this type are AG Peg, HM Sge, V1016 Cyg and V4368 Sgr.

There is a clear disproportion among catalogued SySt in favor of the NB-SySt type, and the known examples of the AO-SySt variety are believed to be just the tip of the iceberg (Mukai et al. 2016). Between 15 and 20 are currently known of the AO-SySt type. Symbiotic stars were originally proposed by Munari and Renzini (1992) as promising progenitors of type Ia supernovae, and the viability of this single-degenerate channel obviously relies on the total number of SySt spread throughout the Galaxy, which in turn heavily depends on the number of AO-SySt. The latter have been usually discovered as counterparts of satellite UV/X-ray sources, while the NB-SySt can be easily spotted at optical wavelengths through the whole Galaxy and the Local Group thanks to their outstanding nebular emission line spectrum (with ionization up to [FeX] and beyond). Most of the NB-SySt have been discovered during photographic objective-prism surveys of the Galactic plane and Bulge (e.g. Merrill & Burwell 1950, Sanduleak & Stephenson 1973, Henize 1976) and many were initially classified and studied as planetary nebulae.

The subtle way the optically-quiet AO-SySt have been usually discovered is well epitomized by the prototype SU Lyn, a V∼8 mag, M6III giant at 650±35 pc distance (Gaia Collaboration et al. 2018). For decades it was a completely unnoticed field star, with just an old report about semi-regular photometric variability which granted it a variable star name. While looking for optical counterparts of hard X-ray sources newly discovered by the Swift satellite, we noted that SU Lyn lied within the error box of one of them: 4PBC J0642.9+5528. Follow-up observations were organized with Swift (to refine the X-ray position) and with Asiago telescopes to investigate if the optical spectra of SU Lyn could betray peculiarities supporting a physical association with the Swift hard X–ray source. The association was proved by a large flux excess observed at bluest optical wavelengths (λ≤4000 Å) and by the presence on high-resolution spectra of weak and variable emission in Hα and [NeIII] lines (Mukai et al. 2016).

The limited sensitivity of current X-ray satellites (soon to change thanks to *e*-ROSITA sky survey) restricts the serendipitous discovery of AO-SySt to those that lie within ∼1 kpc from the Sun, implying that many of their red giants rank among naked-eye objects (like 4 Dra, HR 1105 or *o* Cet). To sample a much larger fraction of the RG in our Galaxy, we have devised a reverse strategy, and first exploratory results are presented in this paper: digging through large spectroscopic surveys in search for the signatures of accretion onto a companion to the RG, primarily the presence of Balmer emission lines having a flux and a profile compatible with an origin in an accretion disk around a degenerate companion. The candidate AO-SySt identified this way can then be subjected to follow-up confirmatory observations, including pointing with X–ray/UV satellites. The GALAH survey of the southern hemisphere (De Silva et al. 2015) offers an ideal opportunity: a large number (aiming at 1 million) of randomly selected southern stars in the $12 \leq V_{JK} \leq 14$ mag range are observed at high S/N and high spectral resolution with the AAO 4m telescope + fibre-fed spectrograph HERMES, over four distinct wavelength ranges that include Hα and Hβ lines.

In this first paper we outline the methodologies guiding our search among GALAH spectra for candidate AO-SySt, report on the discovery of a first batch of 33 new candidate AO-SySt (about doubling the total known so far), and describe the results of a wide range of follow-up observations aiming to confirm their AO-SySt nature. We encourage further observations by the community in order to validate their AO-SySt classification. In this paper we focus on AO-SySt containing giants of the M type. Other spectral types for the cool giant (e.g. Carbon, or G-K) will be explored in follow-up studies.

2 SU LYNCIS, A PATHFINDER

SU Lyn is a prototype for AO-SySt. We intensively observed it in the preparatory phase leading to the discovery paper (Mukai et al. 2016), and kept a tight monitoring afterwards. We have collected a continuous multi-band optical lightcurve, performed runs in search for flickering, revisited it many times with the Swift satellite looking for changes in the X-ray and UV emission, regularly recorded fluxed low-res optical spectra (3300-8000 Å, 2.31 Å/pix), and obtained a great number of Echelle high-resolution spectra (3600-7300 Å, res.pow.=20,000). Such a large amount of information will be digested in detail elsewhere (Munari et al., in prep.), but some partial results can be anticipated here as they provide a guideline for the properties of candidate AO-SySt among GALAH stars that we present in this paper.

The two most obvious distinctive characteristics of optical spectra of AO-SySt are shown in Figure 1: (*a*) a near-UV ultraviolet excess ($\lambda \leq$ 4000 Å), and (*b*) weak emission lines, primarily from the hydrogen Balmer series. They both originate in the accretion disk forming around the degenerate companion, fed by the material accreted from the mass-loosing RG companion.

Both can vary greatly in time, as the two epochs compared in Figure 1 illustrate well: in just over one year SU Lyn passed from an *active* state (Dec 19, 2015), when its SySt nature was quite obvious, to a *quiet* phase (Feb 16, 2017) during which an optical spectrum would have not betrayed its binary nature. This needs to be kept in mind when comparing GALAH spectra with ancillary data taken at widely different epochs.

The most important role of SU Lyn in guiding our search among GALAH stars is however the observed profile for emission lines, Hα in particular. Figure 2 presents a temporal sequence from Asiago 1.82m and Varese 0.84m telescopes + Echelle spectrographs illustrating the great variety of profiles observed for Hα in this star from 2015 to 2020 (for a more traditional presentation of some of these

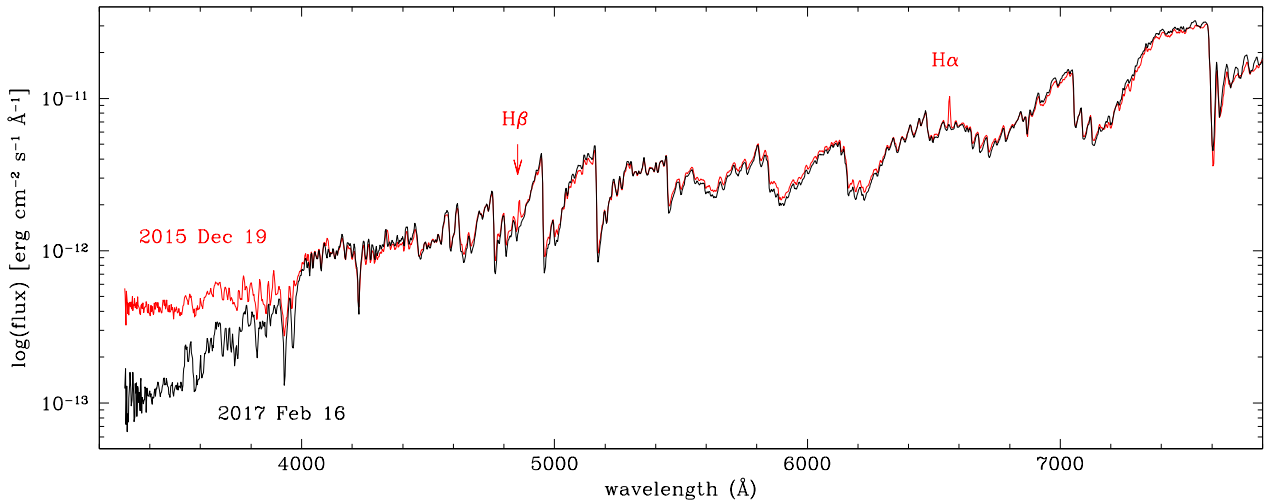

Figure 1. Two spectra of SU Lyn, a prototype of the accreting-only symbiotic stars, to illustrate the differences between low (black) and high (red) accretion rates (Asiago 1.22m telescope). A higher rate causes a brightening of the accretion disk around the white dwarf, which manifests as an excess near-UV brightness ($\lambda \leq 4000$ Å) and detectable emission lines (primarily hydrogen Balmer lines).

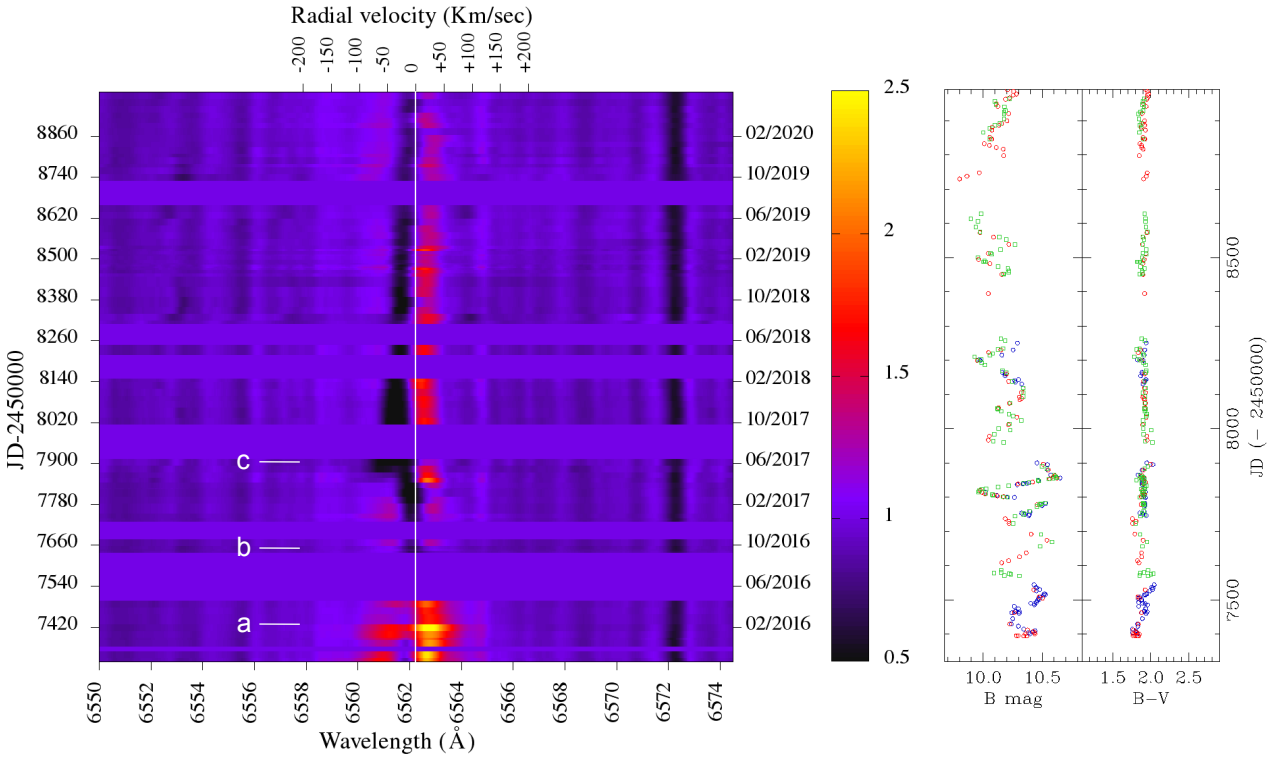

Figure 2. Temporal sequence from Asiago 1.82m and Varese 0.84m Echelle spectra illustrating the great changes observed in the Hα profile of prototype SU Lyn since its recognition in late 2015 as an accreting-only symbiotic star. The vertical line marks the Hα rest wavelength at the stellar systemic velocity (−24 km s^{-1}). The epochs *a*, *b* and *c* are discussed in the text (sect. 2). On the right the corresponding *B*,*V* lightcurve of SU Lyn as built from ANS Collaboration observations.

same profiles for key epochs see Figure 3 of Munari 2019). The orbital plane of SU Lyn is probably close to face-on conditions and this accounts for the negligible changes in radial velocity observed for the M6III absorption lines ($\leq$2 km s^{-1}).

The epoch marked *b* in Figure 2 corresponds to the lowest accretion rate and it is noteworthy for the absence of emission in Hα and a null near-UV excess: at optical wavelengths SU Lyn appears like a normal and single M6III, not as an interacting binary. Only the reduced equivalent width of the Hα absorption (only about half the photospheric value of typical M6III giants) and its narrow FWHM (again half the value for normal M6III giants) could ring a bell. The white vertical line in Figure 2 represents the photospheric velocity of the cool giant: on epoch *b*, the velocity of the Hα absorption almost equals that of the M6III giant. This is not

the case for most of the time, however: as clearly shown by Figure 2, the Hα absorption is normally blue-shifted compared to photospheric absorptions as if originating in a gentle wind blowing off the inner regions of the accretion disk (and thus appearing superimposed onto its emission), or forming in the outer layers of the expanding wind of the RG that engulfs the whole binary system.

Epoch *c* in Figure 2 marks the sudden appearance of a second, distinct and faster moving absorption component, that gradually reduced its velocity during the following months and finally merged with the slower, pre-existing absorption component. At the time of maximum equivalent width of this second absorption component, the emission in Hα briefly vanished.

Finally, epoch *a* represents the condition of highest accretion rate, with a strong near-UV excess and a prominent and structured emission in Hα, with still superimposed the blue-shifted absorption component mentioned above. It is a lucky circumstance that when we first observed SU Lyn in preparation of the Mukai et al. (2016) paper, the star was exhibiting a most prominent emission in Hα and the strongest near-UV up-turn: if at the time, it appeared as in epoch *b* of Figure 2, we could not have recognised it for what it really was.

Another important point illustrated by Figure 2 concerns the photometric activity of SU Lyn. The star is too bright to be recorded unstaturated by surveys which monitor the heaven on a nightly basis in search for transients (eg. ASAS-SN, MASTER, ZTF, etc.), so we monitored it ourselves with small instruments, and fully transformed the observations to the Landolt (1992) standard UBVRI system. As illustrated by the *B*,*V* lightcurve on the right panel of Figure 2 (synchronized to the same temporal ordinates as the spectra to the left), SU Lyn varies by up to 0.7 mag amplitude in a random fashion, with no persistent periodicity. There is no associated change in color and no correspondence with the behavior of the accretion disk as traced by Hα intensity and profile. Thus, the variability is not caused by brightenings and fadings of the accretion disk (vastly hotter than the M6III), but must originate with the cool giant. All cool giants exhibit variability to some extent (Hoffmeister, Richter, & Wenzel 1985; Sterken and Jaschek 2005), given the unstable nature of their convective outer layers and their tenuous atmosphere that extends across the temperatures for molecule formation and through those for dust condensation. The absence of radial velocity variability on the left panel of Figure 2 precludes an origin of the variability seen in SU Lyn with the coherent, large scale, persistent radial pulsations of the type observed in Mira long-period variables. The latter show a sinusoid-like radial velocity curve of ~10-15 km s^{-1} in amplitude, in phase with the equally sinusoid-like lightcurve that can span up to 10 magnitude in amplitude, and characterized by bluer color at maximum and redder at minimum.

The distinction with radially-pulsating giants is important: their outer layers experience large scale motions that lead to shocks, which in turn power emission lines. In our search for AO-SySt we aim to avoid the contamination from radially-pulsating giants and their deceiving emission lines. The various selection steps taken to prune the final AO-SySt sample from as many as possible such false positives are outlined through the rest of the paper.

Table 1. Short and long wavelength limits of the four spectral intervals recorded by the GALAH survey.

interval	start	end
blue	4718	4903
green	5649	5873
red	6481	6739
far red	7590	7890

3 THE GALAH SURVEY

3.1 Motivation

The GAlactic Archaeology with HERMES (GALAH, De Silva, et al. (2015)) is an ongoing spectroscopic survey whose ambitious goal is to unveil the formation and history of the the Milky Way. This is the focus of the field of Galactic Archaeology, which tries to determine how the fossil remnants of star-forming regions and effects of ancient mergers paint the picture of our Galaxy that we observe and measure today. This complex endeavor can be accomplished by studying the detailed chemical composition and other properties of stars in distinct regions of the Milky Way.

The Galactic Archaeology community argues that the complete Galaxy formed gradually over time. This formation history can be traced back by investigating remnants of initial building blocks or subsequent additions through mergers, which have been disrupted in the course of evolution and are now dispersed around the Galaxy. The theoretical concept of chemical tagging (Freeman & Bland-Hawthorn 2002) demonstrates that individual galactic components should have preserved their original chemical signature over time. It is therefore essential to disentangle their formation site from migration history in order to explain the current mixture of stellar populations.

GALAH aims to achieve this by measuring the abundance of up to 31 chemical elements coming from seven independent major groups with different nucleosynthetic origin: light proton-capture elements Li, C, O; α-elements Mg, Si, Ca, Ti; odd-Z elements Na, Al, K; iron-peak elements Sc,V, Cr, Mn, Fe, Co, Ni, Cu, Zn; light and heavy slow neutron capture elements Rb, Sr, Y, Zr, Ba, La; and rapid neutron capture elements Ru, Ce, Nd and Eu (De Silva, et al. 2015).

3.2 Instrument

The goals of the GALAH survey were the main driver for the construction of the High Efficiency and Resolution Multi-Element Spectrograph (HERMES, Barden, et al. (2010); Sheinis, et al. (2015)), a multi-fibre spectrograph working in tandem with the 3.9-metre Anglo-Australian Telescope (AAT) situated at the Siding Spring Observatory, Australia. The spectrograph has a resolving power of R ~ 28,000 (or R ~ 45,000 when slit mask is used) and records spectra in four separate wavelength ranges given in Table 1. The total spectral coverage is therefore approximately 1000 Å, including the important diagnostic lines Hα and Hβ, together with lines of numerous chemical elements that are necessary to fulfil the ambitions of the GALAH survey.

The AAT uses the Two Degree Field (2dF) robotic positioning system with two identical plates that are used to

precisely position fibers at designated locations. This configuration allows HERMES to simultaneously record spectra from up to 392 fibers distributed over a 2° diameter field of the night sky, with an additional 8 fibers used for the telescope guiding. During the exposure with the first plate, the robotic positioner places fibers on the second plate, where each complete process of fibre allocation takes about half an hour per plate. HERMES can typically achieve a signal to noise ratio (SNR) ~ 100 per resolution element at magnitude V=14 in the red arm during a 1-hour long exposure. To achieve as high SNR as possible, minimize atmospheric diffraction, and in order not to loose light due to the fibers' field of view of only 2″, all observations are ideally carried out close to the meridian.

3.3 Selection function

The main selection function of the GALAH survey is relatively simple: it avoids the crowded regions of the Galactic plane ($|b| > 10°$), accounts for the nominal telescope operations ($-80° \leq \delta \leq +10°$) and restricts observations by apparent magnitude ($12 < V_{JK} < 14$), while being color independent. There is an additional requirement for field selection: the density of stars has to be at least 400 per π square degrees to match the number of fibers and field of view of the fibre positioner. The input catalogue for observations is based on the Two Micron All-Sky Survey (2MASS Skrutskie, et al. 2006), with V_{JK} approximating standard V magnitude and being computed as (for more details see Martell, et al. 2017):

$$V_{JK} = K + 2(J - K + 0.14) + 0.382\mathrm{e}^{(J-K-0.2)/0.5} \quad (1)$$

The majority of observations are performed with the above described selection function. Additionally, GALAH employs a bright mode ($9 < V_{JK} < 12$) during twilight or poor observing conditions, and a faint mode ($12 < V_{JK} < 14.3$) when fields with normal or bright configuration are not available to be observed.

The spectroscopic data used in this work is further complemented by observations of the K2-HERMES survey Wittenmyer, et al. (2018) and the TESS-HERMES survey Sharma, et al. (2018), which are carried out with the same observational and data reduction setup as the GALAH survey, albeit with their peculiar selection functions focusing on K2 (Howell, et al. 2014) and TESS (Ricker, et al. 2015) targets, respectively.

Together, the above described observations yield a dataset of 625 757 successfully reduced stellar spectra, of which a small fraction belongs to repeated observations of 600 255 unique stars observed by GALAH at the time of writing of this paper. They represent dwarf as well as giant stars, the former consisting of mostly nearby stars (closer than 2 kpc) while the latter probing distances as far as the Galactic center.

3.4 Data reduction and analysis

Every stellar spectrum recorded by the HERMES spectrograph and used in this work is homogeneously reduced by an automatic reduction pipeline, thoroughly described by Kos, et al. (2017). We hereby provide only a brief explanation of this reduction procedure.

The path from a 2D image recorded in each of the HERMES arms to a one-dimensional, continuum-normalized and zero-RV-shifted spectrum starts with the following steps: raw image cosmetic corrections, spectral tracing, optical aberrations correction, scattered light and apertures cross-talk removal, wavelength calibration, sky subtraction, and telluric absorption removal. Afterwards, spectra are continuum-normalized and shifted into their rest-frame by cross-correlating them with a set of 15 AMBRE model spectra (de Laverny, et al. 2012). This procedure also yields initial radial velocities, while initial stellar parameters ($T_{\rm eff}$, $\log g$, [Fe/H]) are determined by a (larger) grid of 16 783 AMBRE spectra. These, internally also called GUESS parameters, were reported in the first GALAH data release (Martell, et al. 2017). The spectra are then directed to the analysis pipeline with the aim of delivering precise and accurate stellar atmospheric parameters and individual elemental abundances, which constitute the core of results reported in subsequent GALAH data releases.

4 SELECTION STEPS

Our search for AO-SySt among GALAH targets started with isolating the cool giants from the rest. In this paper we focus on giants of the M spectral types, those most abundant (~70%) among the known SySt (see the catalogs by Allen (1984), Belczyński, et al. 2000, and Akras et al. 2019). SySt containing other types of cool giants will be explored in follow-up papers.

4.1 Color

The intrinsic color of M0 giants in the Solar neighborhood is $(J - K)_o$=0.97 (Lee 1970, Koornneef 1983), so we first apply a color selection of $(J - K_s)\geq$0.90 to GALAH targets to both account for the natural spread with the breath of the M0 spectral type and the slight difference in wavelength-baseline between the Johnson's $(J - K)$ and 2MASS $(J - K_s)$ indexes.

4.2 Parallax

On the HR diagram, stars with an M spectral type are either very low-mass main sequence objects (down to the limit for stable H-burning in the core), or giants resulting from the evolution of more massive progenitors. The stars in our Milky Way have not lived long enough to significantly populate the range in between. M-dwarfs are intrinsically very faint and over the $12 < V_{JK} < 14$ mag range covered by GALAH targets, they represent the stars closest to the Sun, while the opposite is certainly true for the giants. In Table 2 we compare (under negligible reddening) the expected parallax of dwarfs and giants with an M spectral type at both ends of the GALAH magnitude range. No giant has a parallax larger than 0.4 mas, or a dwarf smaller than 10mas. Therefore a second criterion was set imposing a Gaia DR2 (Gaia Collaboration et al. 2018) parallax $\pi\leq$3 mas. In this paper we will refer to M *giants* in general, without attempting to distinguish between those of luminosity class III (those

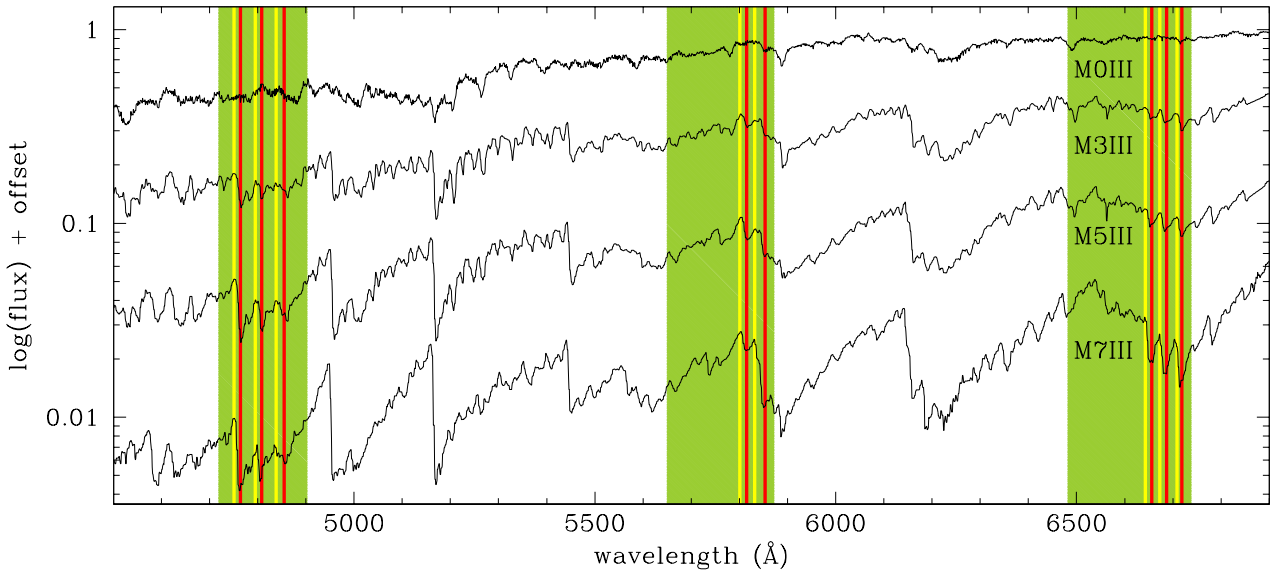

Figure 3. Definition of TiO classification indexes. The shadowed regions show the wavelength ranges covered by the GALAH blue, green and red channels. The yellow and red bands mark the A-B and C-D wavelength intervals, respectively, used to computed the b, g and r ratios according to Eq.(2) and Table 3. In background some Asiago 1.22m spectra illustrating the progress in strength of TiO bands moving along the sequence of M giants (pay attention to the log-scale of the ordinates).

Table 2. Parallax for dwarf and giant M stars (under negligible reddening) at the bright (V=12) and faint (V=14) end of the GALAH magnitude range.

	M_V	parallax (mas)	
		V=12	V=14
M0V	8.90	24	10
M5V	12.30	115	46
M0III	−0.10	0.38	0.15
M5III	−0.90	0.26	0.10

Table 3. Short and long wavelength limits of the intervals used to compute the ratios in Eq. (2) and illustrated in Figure 3.

ratio	λ_A	λ_B	λ_C	λ_D
b1	4751	4756	4765	4770
b2	4798	4803	4807	4812
b3	4835	4840	4850	4855
g1	5801	5806	5812	5817
g2	5829	5834	5850	5855
r1	6641	6646	6653	6658
r2	6670	6675	6684	6689
r3	6706	6711	6716	6721

expected to dominate the sample) and the rarer super-giants of luminosity classes II and I. At the involved distances, Gaia DR2 parallaxes are not accurate enough. This is however of no practical consequence because the results reached in this paper do not depend on such a distinction in luminosity class.

4.3 TiO absorption bands

The above color and parallax criteria combined together returned an initial sample of 29514 GALAH stars. This sample could contain hotter giants of G and K spectral types affected by a large reddening (some of circumstellar origin, or interstellar for objects at the lowest galactic latitudes explored by GALAH) or cool giants of a spectral type other than M (like the Carbon giants). To prune them out and retain only those with a true M-type spectrum, we looked for signatures of their distinctive TiO absorption bands in the GALAH spectra (this could have included also some S-type giants that in addition to absorption bands by molecules involving s-type elements - like the prominent ZrO - still retain TiO absorption bands in their spectra; Turnshek et al. 1985).

Figure 3 presents a progression of M giant spectra with over-plotted in green the wavelength range of the blue, green and red GALAH channels. Within their span lie strong TiO bands, and the later the spectral type, the deeper such bands become. To confirm the presence of the TiO bands and objectively derive their depth, we defined eight narrow TiO wavelength bins (marked in red in Figure 3) and an equal number of control wavelength bins (marked in yellow in Figure 3). The control bins are all placed to the blue of their respective TiO bins given the fact that absorption bands of the TiO molecule all degrade to the red and present a steep band-head to the blue (Pearse and Gaydon 1976). We then defined eight *ratios* (b1, b2, b3 in the blue channel, g1, g2 in the green, and r1 , r2 and r3 in the red) by integrating the flux within the TiO bin and dividing by it the control bin as:

$$\text{ratio} = \frac{\int_{\lambda_A}^{\lambda_B} f(\lambda) d\lambda}{\int_{\lambda_C}^{\lambda_D} f(\lambda) d\lambda} \qquad (2)$$

where the respective wavelength intervals A–B and C–D are listed in Table 3. These ratios were computed on spectra

Table 4. Intervals in combined f-ratio (Eq. 2) defining the template bins for the selected 15824 M giants. $(J-K_s)_\circ$ is the median value within the bin for the reddening corrected $(J-K_s)$ from 2MASS. The last column lists the number of stars in each bin.

bin	left limit	right limit	$(J-K_s)_\circ$	N. stars
00	1.0200	1.0303	0.904	3419
01	1.0304	1.0419	0.935	2309
02	1.0420	1.0561	0.968	1732
03	1.0562	1.0736	0.994	1424
04	1.0737	1.0950	1.017	1282
05	1.0951	1.1214	1.043	1200
06	1.1215	1.1539	1.065	1048
07	1.1540	1.1938	1.088	919
08	1.1939	1.2428	1.110	917
09	1.2429	1.3030	1.141	849
10	1.3031	1.3770	1.166	638
11	1.3771	1.4679	1.182	77
12	1.4680	3.6559	1.139	10

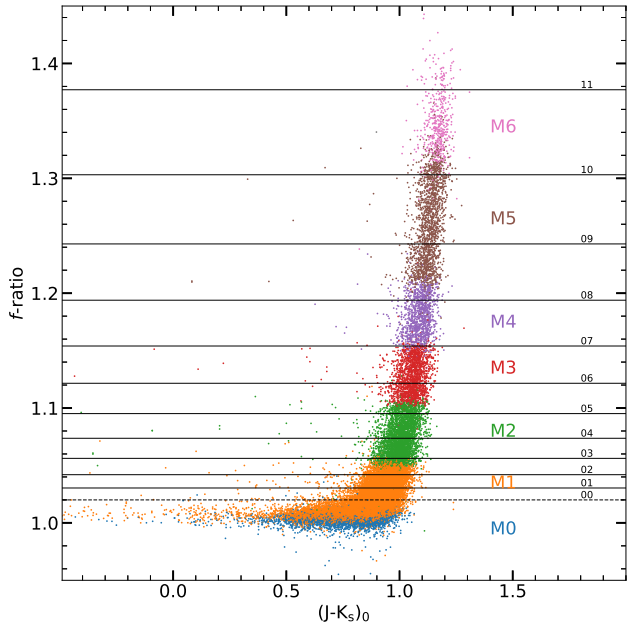

Figure 4. Relation between the reddening-corrected 2MASS $(J-K_s)_\circ$ color index and the combined f-ratio from Eq.(2) for the 29,514 GALAH stars in our initial sample. The colored bands mark the approximate location of the MKK spectral subtypes (M0III, M1III, ...). The finer, log-scale subdivision according to Table 4 is given by the horizontal lines and it is marked by the numbers to the right (00, 01, ...).

before continuum normalisation but shifted to rest frame by the radial velocity listed in GALAH DR3 as rv_guess (Buder et al. 2020, to be submitted). Absence of absorption by TiO returns a value around 1.0 for any of the ratios, and a progressively larger value with increasing M spectral subtype (M0 → M10). Finally, we have combined the eight ratios into a single one computed as

$$f = \frac{[0.3(< b > -1) + 1] + < g > + < r >}{3} \quad (3)$$

where <b> stands for the arithmetic average of b1, b2 and b3, and similarly for the rest. The <b> average ratio stretches over 3.3× the range of the other two, so we have consequently reduced its impact to make it equal to the others. This is justified by the lower S/N of the spectra recorded in the blue channel compared to green and red ones.

The depth of the TiO bands has been already used in the past to classify the M giants of symbiotic stars, for ex. by Kenyon and Fernandez-Castro (1987) that used to this aim the bands at 6180 and 7100 Å(both outside the GALAH wavelength range). In these studies, equivalent widths of TiO bands were measured over their entire wavelength span (hundreds of Å), too wide compared to the breadth of GALAH channels, and therefore inapplicable in the present paper (and for that matter also to more conventional, high-resolution Echelle spectra covering too small a wavelength interval over a single order).

The way our ratios are defined, makes them insensitive to spectral fluxing or continuum normalization issues within the GALAH data reduction process, as well as to reddening. The relation between f-ratio and reddening corrected $(J-K_s)_\circ$ index for the initial sample of 29514 GALAH stars is illustrated in Figure 4. The latter shows a number of highly kreddened stars contaminating the sample. To filter them out we took all stars laying above the knee at f>1.02, and considered the remaining 15824 objects as representing the true M-giants present among the 600 255 stars observed by GALAH at the time of writing of this paper. The $(J-K_s)_\circ$ color index has been calculated from 2MASS photometry and the full extinction as given by Schlafly & Finkbeiner (2011). The choice of taking the full value of the tabulated extinction is justified by considering the great distance to our targets (typically some kpc, where Gaia DR2 parallaxes are inaccurate) and their large galactic latitude, which makes their sight-lines exit the Galactic dust slab well before reaching them.

4.4 Hα in emission

Once the true M giants have been separated from the rest, we searched for those showing Hα (and Hβ) in emission. All the symbiotic stars considered in this paper show Hα emission directly on the recorded spectrum, well before any reference spectrum is subtracted (cf. Figure 5). To properly reconstruct the profile of the emission line, it is however necessary to subtract the underlying spectrum of the M giant. To define the latter, we grouped the M giants by similar strength of TiO bands, and computed the median of the continuum normalized spectra within each bin. The spectral progression of the templates around Hα and Hβ is compared in Figure A1 of the Appendix.

We initially selected to define a unique template for each of the eleven M0 III↔M10 III spectral subtypes of the original MKK classification scheme (Morgan, Keenan & Kellman 1943; Morgan and Keenan 1973), but quickly realized that at the high S/N and high resolution of GALAH spectra, any such subtype spans too wide a range in stellar properties for a single template to adequately represent them all. Similarly, equally spaced bins in f-ratio are not satisfactory, as they oversample at low f values. Therefore, we decided for

a logarithmic progression, with Table 4 listing the 13 final bins, their interval in terms of f-ratio, and the number of true M giants contained in that bin. Their subdivision of the giant branch is shown in Figure 4 (horizontal lines). The median of all the spectra in a given bin defines the template spectrum for that bin. Taking the median value eliminates any disturbance from cosmic ray hits or rare presence of emission components, while averaging over a large number of spectra boosts the S/N (which is already quite high - typically 100 or higher - for a single spectrum), and makes the result insensitive to individual chemical peculiarities.

The template is finally subtracted from continuum normalized spectra of the true M giants within the given bin, and the residuals inspected for emission in Hα. In this first paper we limit ourselves to consider only the M giants showing an Hα emission profile rising above a threshold of 0.5 on the subtracted spectrum. This returned a total of 223 stars.

4.5 Visual inspection

The spectra of these 223 stars were visually inspected for inconsistencies that could cause the Hα to appear in emission on the subtracted spectrum.

Some spectra were found to suffer from a mismatch in radial velocity with the template. In these few cases, the radial velocity rv_guess from GALAH DR3, which is used to shift spectra in all four GALAH channels to rest frame, provides correct results for the blue, green, and infrared, but not for the red channel, resulting in an excess flux around Hα in the difference spectrum, which is obviously spurious.

Another, more frequent cause for false positives was the presence of an emission component originating from the sky background that has not been fully cancelled-out by the sky-subtraction procedure. This may happen e.g. when the target star is located in a region of the sky affected by diffuse background emission, like emission nebulae and HII regions. Such cases are easy to recognize because the Hα and Hβ emission lines are (*a*) typically quite sharp, single-component and symmetric, (*b*) frequently accompanied by [NII] 6548, 6584 nebular emission lines (which do not form in the high density environment of an accretion disk), and (*c*) usually displaced in velocity with respect to the M-giant spectrum by an amount larger than expected from orbital motion in a binary. In multi-fiber spectroscopic surveys like GALAH, only a limited number of fibers are devoted to record the sky background. They are randomly placed over the field of view away from the position of known stars. This is perfectly fine for a great fraction of the sky away from the Galactic plane. There are however, here and there, regions of the sky affected by background emission due to diffuse nebulosity. The intensity of such emission may vary appreciably over limited angular distances, and the same may be the case for the internal nebular gas dynamics and therefore the resulting wavelength for Hα and Hβ emitted lines. Any sparse mapping realized by a limited number of sky fibers of such a complex 2D pattern can naturally result in non-null residuals of the sky-background subtraction, in addition to other caveats of sky subtraction as explained in Kos, et al. (2017).

There was also a group of stars which presented an equal excess *emission* in Hα and Hβ on the subtracted spectrum, always with the same characteristic profile (steep red and blue ends, flat and rounded top), as if originating from an hydrogen deficiency compared with the template spectrum. These stars were also disregarded in the current selection process.

After a few more rejections for miscellaneous reasons, we were left with a final selection of 83 M giants showing genuine emission in Hα with an intensity in excess of 0.5 in the subtracted spectrum (in short the 83-sample hereafter). Stars with an emission in Hα weaker than 0.5, which are inherently more subtle to treat, will be investigated in a follow-up paper.

4.6 Filtering out the radial pulsators

Not all the objects in the 83-sample are necessarily valid AO-SySt. The main false-positive are expected to be the (large-amplitude) radial pulsators (e.g. Miras or SRa variables), that may give origin to emission lines (primarily hydrogen Balmer) deep in their atmosphere where shocks form.

It is of course not precluded that a Mira pairs with a compact companion to form a symbiotic star. For ex. V407 Cyg, prior to its 2010 nova outburst, was studied as a Mira suffering from possible dust-obscuration episodes (Munari, Margoni & Stagni 1990) with little (or none) spectroscopic evidences for binarity (Hinkle et al. 2013). *Mira* itself (= *o* Cet) is a well known AO-SySt: Hubble in the ultraviolet and Chandra at X-rays have spatially resolved its WD companion, the accretion disk and the stream fueling it (Karovska 2006). Such a plethora of multi-wavelength information is however not available for a typical GALAH anonymous star, and to be on the safe side we decided - at the initial stage of our project represented by this paper - to filter out the radial pulsators. Such a pruning is based on converging photometric (lightcurve) and spectroscopic (Hβ/Hα emission ratio) criteria.

We decided not to rely on existing compilations of known variables (as for example collected in the VSX[1] catalog), because the adopted classification criteria (as well as amplitude and periods) are sometimes in (gross) disagreement among themselves and also in conflict with the naming conventions listed in the IAU General Catalog of Variable Stars[2]. We preferred instead to analyze in a homogeneous way their photometric behavior ourselves. To this aim we downloaded the available photometry for the 83-sample from the ASAS-SN sky patrol survey (Shappee et al. 2014, Kochanek et al. 2017) and examine ourselves the resulting lightcurves, which are usually composed by hundreds of individual observations in either g or V bands distributed over a time-interval of a few years, and therefore adequate to reveal the presence of long and stable periodicities related to pulsation. ASAS-SN sky patrol covers the whole accessible sky on both hemispheres every night and the $12 < V_{JK} < 14$ mag range of our targets is ideally placed at the center of ASAS-SN dynamic range, away from the bright saturation limit or the noisy detection threshold.

The lightcurve of a Mira shows regular, long period (from several months to longer than a year) and large amplitude (from a few to >10 magnitudes) sinusoid-like varia-

[1] http://vizier.u-strasbg.fr/viz-bin/VizieR-3?-source=B/vsx/
[2] http://www.sai.msu.su/gcvs/

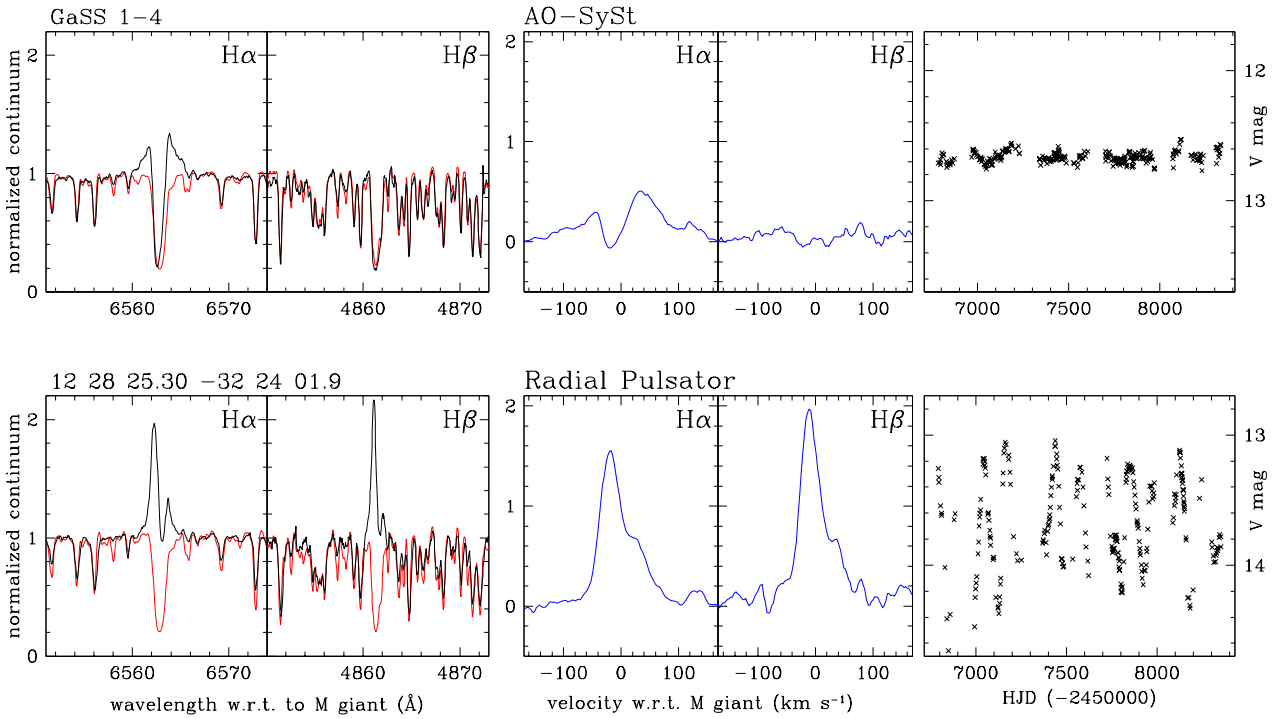

Figure 5. *Left-most panels*: example Hα and Hβ profiles (in black) from RV-zeroed GALAH spectra of a symbiotic star (top row) and of a radial pulsator, compared with those of the template for the same f-ratio bin (in red, cf. Table 4). *Center panels*: the result of subtracting the (red) template spectrum from the (black) object spectrum from the left panels. *Right-most panel*: the corresponding V-filter lightcurve from ASAS-SN sky patrol data.

tions (eg. Hoffmeister, Richter, & Wenzel 1985; Sterken & Jaschek 2005). The large scale radial pulsation is betrayed by the in-phase variation of the radial velocity of the absorption spectrum, with amplitudes of the order of ∼10-15 km/s (Joy 1926; see exemplary Figure 27 of Hoffmeister, Richter & Wenzel 1985). Our pathfinder SU Lyn shows a significant variability (0.6 mag amplitude in V), but it lacks the larger amplitude and the regular beat of a Mira. As clearly illustrated by Figure 2, the M giant in SU Lyn does not radially pulsate in any significant way (the absorption lines are stable in radial velocity to better than 2 km s^{-1}), and therefore no shocks form in the atmosphere which could lead to emission in the Balmer lines. Armed with these consideration, and to stay on cautionary side, we selected to flag on the 83-sample all the stars showing ASAS-SN lightcurves with an amplitude in excess of 0.7 mag and a stable and clean sinusoid-like shape. Such a lightcurve could however arise also from orbital motion, for example from ellipsoidal distortion when the cool giant fills its Roche lobe and/or its side facing the companion is irradiated and heated up (for ex. as in the accreting-only and recurrent nova T CrB; Munari, Dallaporta & Cherini 2016). A spectroscopic confirmation of the radially pulsating nature is therefore required, and this needs to be accommodated within the single-epoch spectra (i.e. no revisit) of the GALAH survey.

In radially-pulsating cool giants, outward moving material collides against the gas lifted during the previous cycle and now falling back inward. The resulting shock is hot enough to excite emission in the Balmer lines of hydrogen. Such shocks develop deep within the atmosphere, interior to the outer layers where absorption by TiO molecules occurs. The absorption by TiO begins around 4200 Å and, by superposition of successive bands (they all decline toward the red), their combined absorption grows rapidly stronger with wavelength (Fluks et al. 1994). As a consequence, emission in Hδ (4101 Å) and higher Balmer terms exit the atmosphere unscathed by TiO, and their flux decline with increasing upper n-quantum number in the usual way. What happens to the red of Hδ? Going from Hγ to Hβ and then Hα, we move into deeper and deeper overlapping absorption by TiO bands and the *observed* emission in the line becomes more and more absorbed. Saying it a different way (Joy 1926; Yamashita, Nariai & Norimoto 1977), in pulsating M giants the strongest line is Hδ and the intensity of successive Balmer emission lines declines *either* going to the blue or to the red (see exemplary spectrum for LQ Sgr presented by Bragaglia et al. 1995). In most astrophysical environments, the observed emission in Hα is invariably stronger than in Hβ, while in Miras the opposite is the case (Merrill 1940), because of the TiO absorption in the outer atmospheric layers. This offers a clear distinction between the emission originating from the accretion disk in an AO-SySt (in terms of equivalent widths: EW(Hα) > EW(Hβ)) from that expected to come from the internal shock regions of an M-type radial pulsator (EW(Hα) ≤ EW(Hβ)).

GALAH high-resolution spectra show a further distinction between the two types. In AO-SySt systems, a sharp absorption component appears superimposed to the broad Hα emission profile, blue shifted by about 5–25 km s^{-1} and twice narrower than the photospheric Hα absorption line (FWHM∼15–25 km s^{-1} as opposed to 45–50 km s^{-1}), that - by analogy with the prototype SU Lyn - is believed to

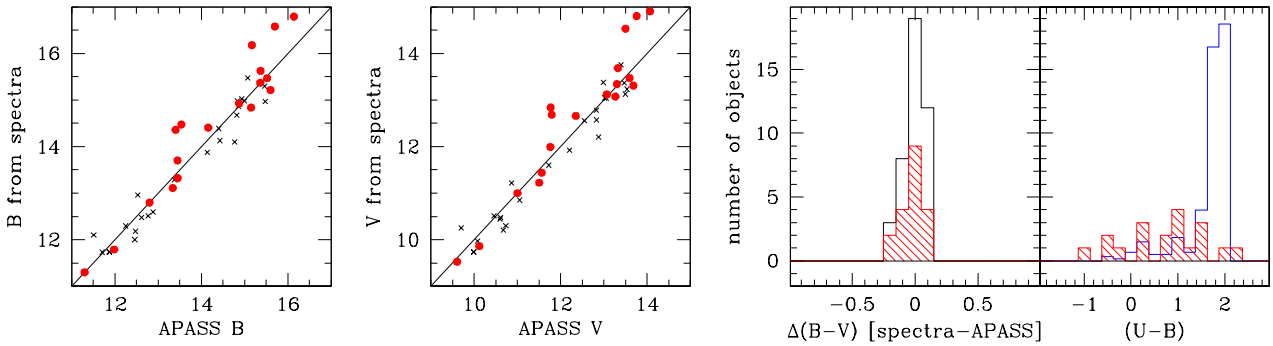

Figure 6. *Left-most panels*: comparison between the average B and V magnitudes from APASS all-sky survey, and the corresponding values derived from Asiago 1.22m flux-calibrated spectra for a subset of the 53-sample. The solid lines mark the 1:1 relation. *Right-most panels*: histogram distribution of differences between Asiago and APASS derived $B{-}V$ colors, and distribution of $U{-}B$ colors derived from Asiago spectra. The line in blue shows the distribution of a hundred M giants from the Solar neighborhood as measured by Fluks at al. (1994). Red color refers to symbiotic stars discovered in this paper, black to other GALAH M giants observed along with them (including also some radial pulsators).

originate in the gentle wind blowing off the accretion disk or in the outer layers of the RG wind that engulf the whole binary system. In the GALAH spectra of radially pulsating stars, the narrow absorption superimposed to the emission is instead generally red-shifted as if coming from cooler material falling back toward the star after being lifted higher up during the previous pulsation cycle.

These photometric and spectroscopic criteria to separate AO-SySt and radially pulsating objects in the 83-sample are illustrated in Figure 5, which presents line profiles and lightcurves well typical of the rest of the sample: high-amplitude and regular beating for the lightcurve of a pulsator, with strong Hβ and red-shifted narrow-absorption; lower amplitude and less regular lightcurve for the AO-SySt, an Hβ much weaker than Hα and blue-shifted narrow-absorption. By applying these criteria, 30 radial pulsators are pruned from the 83-sample, reducing the candidates AO-SySt to 53. Hereafter, we refer to them as the 53-sample.

5 THE SELECTED 33 AO-SYST

We have finally subjected the sample of 53-sample to a series of follow-up observations from the ground and space to pick-up the most promising objects. Based on their results, our final list of 33 proposed candidates AO-SySt is presented in Table 5 (where GaSS in their names stands for Galah Symbiotic Star); they are divided in two groups, those of higher confidence and the rest. A plot similar to Figure 5, presenting the Hα, Hβ profiles and the lightcurve, is provided in the appendix for all 33 objects (Figures A2–A8). We now describe the follow-up observations that have led to the compilation of Table 5. A complete description of such extensive follow-up observations is far beyond the scope and breadth of the present paper. Full details, augmented by the results of further follow-up observations currently in progress, will be presented in a separate paper.

5.1 Near UV up-turn

The presence of a bright accretion disk is betrayed by an emission excess at wavelengths shorter than ~4000 Å, as illustrated for SU Lyn in Figure 1. With the long-slit B&C spectrograph attached to the Asiago 1.22m telescope, highly efficient down to the atmospheric cut-off (~3200 Å at the 1000m above sea level location) we have observed most of the object in the 53-sample located north of −29° in declination (Table 1A in the Appendix provides a log-book of these observations). At the Asiago +46° latitude, this corresponds going down to just 15° degrees over the horizon. The near-UV faintness of the program stars and the high atmospheric extinction at such large air-masses conjured to make such observations quite demanding to execute. A consistent number of spectro-photometric standards were observed in parallel each night at similarly high air-masses. Suitably high S/N at 3400-3600 Å was obtained for only a fraction of the attempted objects, and sometimes only after adding spectra collected at different revisits. The objects marked "spc" in the $U_{\rm exc}$ column of Table 5 are those showing excess emission on spectra over the range $3400{\le}\lambda{\le}4000$ Å(cf. equivalent SU Lyn spectra presented in Figure 1). There are clear hints for some of them that the amount of near-UV excess changes when spectra taken at different epochs are compared.

A quick summary of the photometric data extracted from spectra is presented in Figure 6. The B and V data lie well on a 1:1 relation with APASS mean data, the scatter being at least in part related to the variability all objects display (as per column ΔV of Table 5). The difference in the $B{-}V$ color (indicative of the accuracy of the *slope* of fluxed spectra) between APASS and spectra appears well distributed around 0.0 with a FWHM of about 0.1 mag. The most interesting panel of Figure 6 is the last one, showing the distribution of $U{-}B$ measured on spectra compared with the distribution of $U{-}B$ for a hundred M giants of the Solar neighborhood (suffering from negligible reddening) as measured by Fluks et al. (1994). It is clear how, on average, the $U{-}B$ color of candidate AO-SySt is bluer that those of (supposedly) single, normal M giants, supporting the notion that for a sizeable fraction of them we have actually observed an excess in U as coming from the companion and the accretion disk. The AO-SySt scoring an "spc" in Table 5 are those with an $U{-}B$ bluer than +0.4 in Figure 6, and "spc:" for those between +0.4 and +0.8.

Table 5. The candidate accreting-only symbiotic stars (AO-SySt) discovered in this paper based on spectra from the GALAH survey. E(B-V) is from Schlafly & Finkbeiner (2011). The spectral type is on the MKK scale and the f-ratio is from Eq. 3 (see sect. 4.3) V is from the APASS catalog. ΔV is our estimate of the amplitude of variability on ASAS-SN sky patrol data (sect 4.6). 'P orb' lists possible orbital periods (for 2×P alternative see sect. 5.6). 'dist' is the distance (in kpc) derived from E(B-V), V and 'spec type' assuming a luminosity class III (Sowell et al. 2007; it is a lower limit to distance for brighter luminosity classes). $RV_\odot$ is from GALAH DR3 (rv_guess). Objects marked 'var' in the 'Asiago RV' column show a variability in radial velocity (cf. Table 6 and sect. 5.2). The column 'Swift' marks with 'X' the objects counterpart to X-ray sources in the 2SXPS catalog (Evans et al. 2019), and with 'UV' those found emitting in the ultraviolet UVM2 band in our Swift follow-up observations (cf. Table 8 and sect. 5.5). U_{exc} lists the presence of emission excess at U-band wavelengths: 'pht' from photometric UBV observations (Massey 2002), 'spc' from our spectra (sect. 5.1). An 'F' in the 'Flk' column marks the presence of flickering (sect. 5.4). The final two columns provide the velocity (w.r.t. M giant) and the FWHM of the narrow absorption superimposed to the broader Hα emission (sect. 4.6).

name	RA (J2000)	DEC	Galactic long	Galactic lat	E(B-V) (mag)	spectral type	f	V (mag)	ΔV (mag)	P orb (days)	dist (kpc)	$RV_\odot$ (km/s)	Asiago RV	Swift	U_{exc}	Flk	Hα (wind) RV (km/s)	Hα (wind) width (km/s)
main sample																		
GaSS 1-1	04 40 35.65	−70 52 42.7	282.3	−35.1	0.23	M1	03	12.950	0.23		3.4	+264.28			pht	F	−21.9	19
GaSS 1-2	05 12 09.82	−70 04 17.6	281.4	−34.4	0.33	M2	04	12.725	0.43		2.9	+234.29			pht		−23.9	19
GaSS 1-3	06 39 21.17	−59 22 26.9	268.7	−26.7	0.04	M0	00	12.521	<0.05		3.2	+282.99		X			−2.1	24
GaSS 1-4	11 07 15.48	−32 12 19.3	279.6	26.2	0.10	M1	00	12.638	0.11	235	3.5	+141.44					−11.3	19
GaSS 1-5	11 21 10.22	−29 22 12.5	280.5	29.6	0.05	M2	02	13.469	0.33	311	6.1	+35.75					−7.4	21
GaSS 1-6	14 53 07.03	−37 46 38.7	326.6	19.6	0.06	M3	05	12.096	0.30	401	3.3	+33.35					−12.3	17
GaSS 1-7	14 48 25.03	−24 57 24.8	336.0	29.8	0.13	M1	02	13.497	0.35		5.0	−235.14			spc		−9.3	24
GaSS 1-8	15 43 54.79	−29 23 14.9	338.3	22.4	0.45	M1	00	13.637	0.16	224	2.9	−143.10					−17.1	24
GaSS 1-9	16 09 28.75	−03 55 45.0	15.7	23.9	0.27	M1	02	13.299	0.28		3.7	−131.58	var:		spc	F	−7.2	11
GaSS 1-10	17 29 24.58	−58 07 21.7	331.4	−10.6	0.15	M1	02	12.568	0.21		3.0	−100.12				F	−4.5	22
GaSS 1-11	17 22 33.15	−47 50 40.4	344.5	−10.2	0.14	M3	06	12.182	0.09	453	3.1	+58.19		UV		F:	−22.0	27
GaSS 1-12	18 16 06.98	−22 57 56.1	13.4	−11.1	0.22	M4	07	11.761	0.85		2.4	+51.88	var	UV	spc:		−11.4	14
GaSS 1-13	19 21 26.71	−07 27 02.4	30.4	−11.3	0.32	M1	01	13.681	0.20	328	4.1	−373.27	var		spc	F	−13.5	19
GaSS 1-14	20 27 56.95	+00 37 53.7	46.2	−23.2	0.06	M2	05	13.019	0.52	381	4.8	−247.79			spc:	F	−6.4	21
GaSS 1-15	21 02 01.51	+04 10 35.4	54.3	−28.2	0.08	M2	04	12.054	0.09	229	3.0	+49.94	var	X		F	−8.1	22
additionary sample																		
GaSS 1-16	05 42 40.32	−66 31 40.2	276.7	−32.6	0.10	M1	02	13.415	0.09		5.0	+302.18				F	−17.7	25
GaSS 1-17	07 41 36.52	−58 06 12.7	269.1	−21.0	0.09	M1	00	11.439	0.24		2.0	+119.77					−2.4	24
GaSS 1-18	12 16 19.12	−38 08 37.7	293.7	23.8	0.06	M1	02	13.068	0.33	338	4.5	+164.65					−16.9	26
GaSS 1-19	14 36 11.36	−78 37 33.9	308.2	−16.8	0.11	M1	01	13.422	0.15		5.0	+247.20					−7.1	26
GaSS 1-20	16 28 54.84	−16 00 32.5	355.0	26.6	0.25	M1	00	12.116	0.59		2.2	+44.76	var				−10.2	17
GaSS 1-21	16 37 42.83	−20 12 23.6	353.8	21.7	0.29	M4	06	13.757	0.70		5.4	−182.82			spc	F	−0.3	18
GaSS 1-22	16 09 17.67	−25 14 20.4	350.5	18.4	0.27	M1	00	11.907	0.32		1.8	−242.25					−8.2	31
GaSS 1-23	17 14 24.39	−12 11 19.9	9.8	15.7	0.44	M4	07	13.321	0.68		3.1	−167.23			spc		−4.6	22
GaSS 1-24	17 38 44.36	−61 17 05.3	329.5	−13.4	0.09	M6	11	13.000	0.75		5.5	+171.01					2.5	19
GaSS 1-25	17 47 59.65	−17 18 37.5	6.1	11.1	0.23	M0	00	11.561	0.17		1.4	−81.87				F	−5.4	29
GaSS 1-26	18 07 34.98	−42 47 42.3	350.0	−10.6	0.10	M3	05	13.508	0.32		6.0	−1.74					−10.3	25
GaSS 1-27	18 00 00.28	−46 32 36.9	348.9	−16.0	0.06	M1	00	11.113	0.29	400	1.8	−42.51					−5.5	14
GaSS 1-28	19 19 02.81	−27 01 19.0	9.1	−14.0	0.20	M2	04	13.265	0.63	496	4.5	−106.75			spc		−4.8	21
GaSS 1-29	19 44 07.66	−47 08 06.7	349.4	−22.4	0.07	M2	04	14.585	0.33		9.6	+149.28					−4.3	23
GaSS 1-30	19 10 35.88	−35 11 50.8	2.4	−19.0	0.07	M0	00	11.120	0.21		1.6	−48.38					−6.1	20
GaSS 1-31	19 02 16.24	−22 17 53.2	15.6	−15.3	0.10	M1	02	11.505	0.54		2.1	+70.13	var:				−2.6	14
GaSS 1-32	19 15 43.66	−29 18 29.8	8.8	−18.3	0.11	M1	01	11.444	0.21		2.0	−95.48					−10.1	23
GaSS 1-33	22 18 02.95	−06 10 07.2	53.9	−46.4	0.05	M1	02	15.434	0.41	682	13.5	−205.14			spc	F	−11.7	15

5.2 Radial velocity variability

Armed with evidence from Figure 2 that the low amplitude, irregular variability affecting the M giant in SU Lyn does not reverberate into changes in radial velocity, we observed some of the 53-sample north of −25° in declination with the Echelle spectrograph mounted on the Asiago 1.82m telescope. As a check, some normal stars from the initial sample of 15,824 GALAH true M-giants were observed and also a few radially pulsating M stars. The results are presented in Table 6. The quoted error for Asiago RVs is the *internal* error, i.e. that derived by comparing the RV obtained from different Echelle orders by cross-correlation with spectra of IAU radial velocity standards of M spectral type. We selected to limit the measurement to 5 of the 32 orders covered by the Asiago Echelle spectrograph, favoring those at redder wavelengths (where S/N is higher), and avoiding the orders with TiO band-heads or telluric atmospheric absorptions that would affect the cross-correlation results. A comparison of Asiago RVs with the GALAH rv_guess and Gaia data in Table 6 returns a +0.5 km s^{-1} offset and an rms of 1.9 km s^{-1}. A similar rms affects the GALAH vs Gaia comparison.

From the GALAH and Asiago RVs in Table 6, a clear RV variability has been observed for four objects, and borderline for additional two. They are marked with "var" in column "Asiago RV" of Table 5. We favor an interpretation in terms of orbital motion for this RV variability.

Table 6. Heliocentric radial velocity of GALAH stars measured with the Asiago 1.82m telescope + Echelle spectrograph compared with the corresponding values of rv_guess listed in GALAH DR3. The mean radial velocity listed in Gaia DR2 is also given, with its formal error and the number of epoch transits over which it has been computed.

		Asiago 1.82m Echelle			GALAH DR3			Gaia DR2		
		UT middle	$RV_\odot$ (km/s)	err (km/s)	UT middle	$RV_\odot$ (km/s)	err (km/s)	$<RV_\odot>$ (km/s)	err (km/s)	N
GaSS 1-9		2020-07-04 22:30	−129.56	0.51	2017-04-09 17:56	−131.58	0.41	−133.07	0.60	13
		2020-10-03 17:49	−130.54	0.15						
GaSS 1-12		2019-09-11 19:13	61.61	0.48	2017-06-04 15:59	51.88				
		2020-07-05 23:15	56.72	0.21						
		2020-10-03 18:10	55.07	0.40						
GaSS 1-13		2020-07-04 22:54	−357.39	1.41	2014-06-11 16:08	−375.27	0.50	−374.54	1.54	4
		2020-10-03 18:51	−373.04	0.18						
GaSS 1-15		2020-09-03 21:21	46.90	0.29	2017-09-06 12:14	49.94	0.29			
		2020-10-03 19:47	51.58	0.04						
GaSS 1-20		2020-07-05 21:03	13.45	0.48	2017-06-03 13:27	44.76	0.43	9.36	0.82	10
GaSS 1-21		2020-07-05 20:42	−181.89	1.70	2015-04-29 13:47	−182.82	0.47	−182.22	0.59	9
GaSS 1-23		2020-07-05 21:45	−166.39	0.92	2016-08-16 09:36	−167.23	0.45	−169.53	1.01	10
GaSS 1-31		2020-07-05 23:36	70.09	0.15	2017-11-06 10:00	70.13	0.51	68.02	0.82	7
		2020-10-03 18:27	71.42	0.16						
		2020-10-17 18:20	69.22	0.72						
GaSS 1-33		2020-10-03 19:10	−206.47	0.36	2014-07-08 17:31	−205.14				
RA	DEC	*radial pulsators*								
20 37 56.95	00 27 53.7	2020-10-03 20:04	−246.87	0.19	2016-08-13 12:56	−247.79	0.40	−250.47	0.61	10
23 31 17.83	−00 30 39.4	2019-12-09 18:30	−34.17	0.49	2017-07-24 17:27	−37.11	0.37	−35.81	0.93	6
		2020-01-15 17:06	−35.67	0.33						
		other GALAH M giants								
03 40 25.30	14 30 00.6	2020-01-13 20:42	11.96	0.21	2016-01-10 10:47	9.94	0.48	9.45	0.70	6
05 21 50.50	01 51 26.8	2019-12-07 01:50	−16.04	0.29	2015-08-30	−14.65		−16.44	1.84	6
		2020-01-13 20:56	−16.97	0.10	2015-12-27 13:09	−12.42	0.31			
06 19 12.30	−17 35 20.8	2020-01-13 22:17	121.64	0.43	2017-01-06 13:35	120.96	0.40	121.47	0.80	7
10 00 41.60	−21 35 54.7	2020-04-10 20:13	188.95	0.58	2016-04-24 09:55	189.81	0.61	191.32	1.02	6
10 32 55.50	12 51 30.4	2020-04-10 20:34	132.82	0.12	2017-02-05 15:42	131.48	0.39	135.27	1.79	3
10 51 30.19	00 43 59.5	2020-04-10 21:04	166.41	0.36	2017-01-27 14:10	163.82	0.33	163.32	0.82	2
12 08 10.13	−09 07 52.8	2020-04-10 21:50	45.84	0.22	2016-04-03 12:48	47.24	0.33	45.68	0.43	20
12 16 50.58	−06 31 19.3	2020-04-10 22:04	83.64	0.19	2017-01-31 15:22	81.32	0.63	83.23	0.32	28
17 19 00.39	−17 45 42.9	2020-07-05 21:21	−23.06	0.91	2017-05-09 15:29	−23.62	0.61			

5.3 Emission line variability

As observed in SU Lyn (cf. Figures 1 and 2), also the AO-SySt of this paper show a clear variability of the intensity and profile of Hα emission line on spectra collected with the Asiago 1.22m and 1.82m telescopes. An example is presented in Figure 7. GaSS 1-31 showed a clear emission in Hα on the GALAH spectrum recorded on Apr 9, 2017, a weaker one on the Asiago spectrum for Oct 2, 2020, and no emission on Jul 5, 2020 (see also sect. 5.5 below) and on Oct 17, 2020 (this last spectrum has been obtained at a lower resolving power (12,000 because of 2×2 CCD binning) with an Echelle spectrograph mounted on the Varese 84cm telescope). The Hα of GaSS 1-12 has been always observed in emission on all three visits with the Asiago 1.82m, with a varying degree of intensity and velocity of the emission relative to the M giant. Most interestingly, the last Asiago spectrum for Oct 3, 2020 shows the appearance of a second narrow absorption, blue shifted with respect to the primary one, an event reminiscent of what happened to SU Lyn in 2017 (cf. Figure 2).

5.4 Optical flickering

The accretion process in binaries is characterized by chaotic processes (e.g. density fluctuations in the accretion flow from the donor to the accreting star) that develop on time scales much sorter that the orbital one, leading to a chaotic photometric variability superimposed on other sources of more regular (and slower) variability like orbital motion (in the form of reverberation, eclipses, ellipsoidal distortion, etc.) or intrinsic to one of the binary components (like pulsation, rotation of a spotted surface, etc.). The fast (seconds to minutes) chaotic photometric variability is usually referred to as *flickering* and it is generally assumed to originate primarily from the hot spot (where the accretion stream impacts the outer rim of the accretion disk) or from the inner and

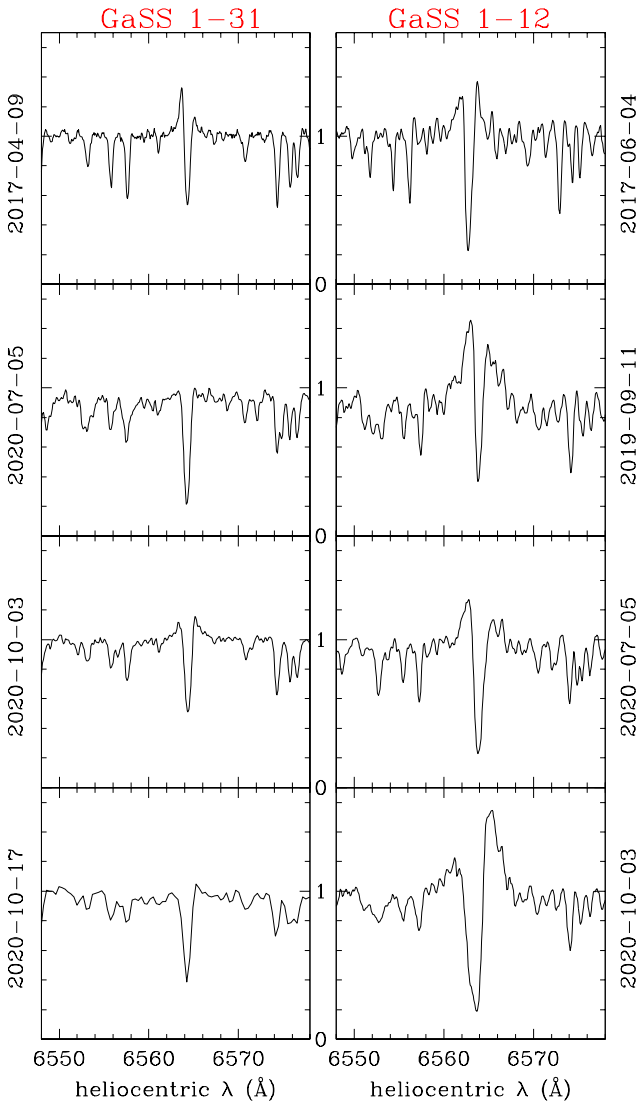

Figure 7. Example of variability observed on Hα comparing the original GALAH spectra (top row) with Asiago 1.82m Echelle spectra obtained at later epochs (the left-bottom spectrum is from Varese 84cm telescope). Only GALAH spectra are corrected for telluric absorption lines.

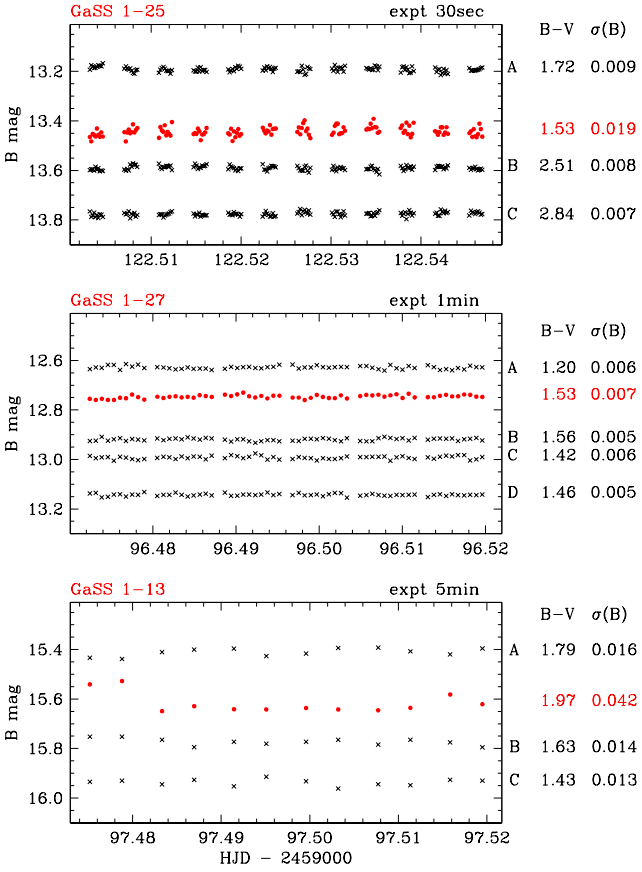

Figure 8. Examples of the *B*-band time series collected on the program stars, with 30sec, 1min and 5min sampling time (from top to bottom), in search for flickering from the accretion disk. The regular gaps correspond to the acquisition of *V*-band frames for the calibration of color equations to transform data to the standard Landolt system. The measured *B*−*V* color of the symbiotic star (in red and filled circles) and of nearby field stars of the similar brightness and color (in black and crosses), is marked to the right, together with the dispersion around the median of the plotted *B*-band data. Symbiotic stars on the top and bottom panels clearly show flickering well in excess of the noise affecting field stars, while that on the center panel is constant at the same noise level of the field stars.

hotter regions of the accretion disk (cf. Warner 1995). The detectability of flickering on optical photometric data depends primarily on its contrast with the steady sources in the system: the fainter the two components of the binary, the easier for flickering to become observable (e.g. Hellier 2001). Therefore, if flickering is easy to observe (amplitude of a few tenths of a magnitude on time scales of seconds) in cataclysmic variable stars that radiate about 1 $L_\odot$ at optical wavelengths, it is an entirely different matter for symbiotic binaries in which the optical luminosity of the cool giant alone counts for 10^2 $L_\odot$.

The regions in the disk responsible for flickering are hot, and their emission is consequently rising toward the blue. That of the giant rises instead toward the red (eg. Skopal et al. 2020). Therefore, to reduce the background glare of the giant it is convenient to go as blue as possible. Detection of flickering at satellite ultraviolet wavelengths is straightforward as demonstrated by the Swift observations of SU Lyn by Mukai et al. (2016). On ground-based observations, the bluest photometric band is *U* (in its many variants, primarily Landolt's or Jonhson's *U*, *u* from Stromgren, or the *u′* from SLOAN photometric system and its derivatives). *U* band was relatively easy to observe at the old times of photo-electric photometers mounted on all-reflecting telescopes with bare-alluminium surfaces, thanks to the high instrumental throughput (no coatings or refractive components) and the excellent sensitivity of photo-multipliers like the standard 1P21 or 31034A. Many searches for flickering in symbiotic stars were performed at that time (e.g. Slovak & Africano 1978; Mikolajewski et al. 1990; Tomov et al. 1996). The advent of CCDs, with their much lower sensitivity at *U*-band wavelengths, badly affected the study of flickering, with rarer attempts performed (e.g. Dobrzycka, Kenyon, & Milone 1996; Sokoloski, Bildsten, & Ho 2001; Zamanov et al. 2011). To further complicate the matter, the sensitiv-

Table 7. *B* and *V* photometry of the candidate AO-SySt as measured during the search for flickering. The given HJD is the middle UT of the 70min duration of the time-series photometry.

	HJD (-2459000)	*B* (mag)	*V* (mag)
GaSS 1-1	117.834	14.248	13.078
GaSS 1-2	117.878	14.374	12.899
GaSS 1-3	102.882	14.067	12.497
GaSS 1-9	94.496	15.429	13.321
GaSS 1-11	95.543	13.825	12.083
GaSS 1-12	96.546	13.874	12.122
GaSS 1-13	97.497	15.605	13.641
GaSS 1-14	129.530	14.792	12.976
GaSS 1-15	97.549	13.838	12.092
GaSS 1-16	124.865	15.125	13.385
GaSS 1-17	120.852	13.137	11.419
GaSS 1-21	130.986	15.921	14.010
GaSS 1-23	94.546	15.419	13.301
GaSS 1-25	122.525	13.441	11.541
GaSS 1-27	96.496	12.746	11.213
GaSS 1-28	128.526	15.415	13.566
GaSS 1-30	124.526	12.964	11.213
GaSS 1-31	125.504	13.007	11.193
GaSS 1-32	126.502	13.336	11.473
GaSS 1-33	130.531	17.076	15.403

ity of CCDs extending up and beyond 1 μm allow signal to be recorded from the red-leak affecting most $U/u/u'$ filters, especially those of the multi-layer dielectric type. Such a red-leak may be so severe with cool giants, that the fraction of recorded photons coming through the red-leak easily outnumber those going through the proper transmission profile of the *U*-band (Munari and Moretti 2012).

To search for flickering among our candidate AO-SySt we used a 50cm telescope, with a 40arcmin well corrected field of view and quality photometric filters, operated robotically for ANS Collaboration in Atacama (San Pedro Martir, Chile). For the above described limitations, we selected to search for flickering in *B*-band, with interspersed observations in *V*-band serving to construct the *B*−*V* color base for the transformation from the instantaneous local photometric system to the Landolt's standard one. Local photometric sequences were extracted from the APASS multi-epoch, all-sky *BVgri* photometric survey (Henden et al. 2016) in its DR8 version.

Given the much brighter emission of the M giant in *B* compared to *U*, the expected amplitude of observable flickering decreases to (at most) a few hundredths of a magnitude. To be detected, such a tiny amount of variation requires highly accurate observations and careful data reduction, under clear and stable skies as usually enjoyable in Atacama. We adopted integration times in *B* of 30sec for the brightest targets and 5min for the faintest, with 60sec for the bulk of objects. Every 10 exposures in *B*, one was obtained in *V* to compute the coefficients of the transformation color equations. The procedure was repeated identically for 70min for each program star. The photometry was performed for most objects in aperture mode, their high galactic latitudes implying sparsely populated fields and therefore no need to revert to PSF-fitting, which was instead necessary for three targets. On average, the 50 field stars closest on the image to the symbiotic star, of a similar magnitude and well isolated from neighbouring stars were also measured on all recorded images in exactly the same way as the symbiotic star. The photometry of these 50 field stars was then inspected looking for those with a *B*−*V* color as close as possible to the symbiotic star in the center. Typically 5 such stars were found, with a few cases scoring just 2 and others up to 8. These field stars with magnitude and color closely matching those of the symbiotic star, serve as perfect samplers of the observational noise above which the flickering has to be detected.

The program AO-SySt subjected to the search for flickering are listed in Table 7, together with the HJD of the central image for the 70min time series, and the average of *B* and *V* measured magnitudes during such time series. The error of such *B* and *V* data is totally negligible in its Poissonian component, while the amount due to transformation from the local system to the APASS one (closely adherent to Landolt's) is systematic and constant for a given object and amounts on average to 0.008 mag (which obviously cancels out when comparing data within a given time-series).

An example of the collected data is presented in Figure 8, with one object each for the 30sec, 1min and 5min sample times. At the top and bottom panels we show objects with a clear detection of flickering well in excess to the noise affecting the field stars, while in the center we see a non-flickering symbiotic that remains stable at a few millimag level through the 70min monitoring. The objects for which flickering was detected well above observational noise are marked with an 'F' in the 'Flk' column of Table 5.

5.5 Satellite X–ray/UV observations

The presence and nature of the accreting source in AO-SySt systems, either a WD or a NS, is best defined by satellite observations performed in the ultraviolet and X–rays, where the peak of the emissivity for accretion-induced processes is located (e.g. Masetti et al. 2007 and references therein, and also Kuranov & Postnov 2015 for a recent review). The X–ray/UV properties of the AO-SySt prototype SU Lyn have been investigated by Mukai et al. (2016) and Lopes de Oliveira et al. (2018) based on observations with *Swift* and *NuSTAR* satellites. They found SU Lyn to show (i) a large (by a factor of a few hundred in flux) UV excess with respect to a 'normal' red giant; (ii) long-term (months to years) hard X–ray variations by an order of magnitude between low- and high-level states in the 15–35 keV hard X–ray emission; (iii) fast UV variability during the high X–ray states (flickering). In the latter ones, the average X–ray flux was $\sim 10^{-11}$ erg cm^{-2} s^{-1} in the 0.3–50 keV band, with the spectrum modelled with a thermal plasma of temperature $kT \sim 20$ keV, plus a fluorescent iron emission at 6.4 keV, absorbed by a hydrogen column N_H as large as $\sim 3\times 10^{22}$ erg cm^{-2}. This absorption has however little effect on the UV excess observed from this source. At a distance of 650 pc, this corresponds to unabsorbed X-ray luminosities of up to $\sim 10^{33}$ erg s^{-1} in the high state, and a factor of 10 larger in the UV. The passage from low- to high-level states in the UV and X-ray emission is attributed to large excursions in the transfer and accretion rates.

In anticipation of a devoted observing campaign, we

Table 8. Results of the *Swift* XRT and UVOT observations of some of the AO-SySt presented in this paper. The fluxes are in units of 10^{-13} erg cm^{-2} s^{-1}. The bottom three objects are radial pulsators observed for comparison. The data for 20 35 04.52 −05 47 35.3 include also additional 485sec exposure obtained on 8 Sep. 2019.

name / RA,DEC	Obs. date	Start time (UT)	XRT obs. duration (s)	0.3–10 keV count rate	0.3–10 keV flux	UVOT obs. duration (s)	UVM2 mag.
GaSS 1-11	13 Jun. 2020	12:05	1885	<3.0e-3	<2.6e-13	1864	17.10±0.06
GaSS 1-12	16 Sep. 2019	00:02	1516	<3.2e-3	<2.8e-13	1701	16.04±0.04
GaSS 1-31	14 Jun. 2020	01:01	839	<3.7e-3	<3.3e-13	830	>19.69
05 11 30.88 −61 29 03.6	10 Jun. 2020	06:31	1973	<1.7e-3	<1.5e-13	1948	>20.42
20 06 56.32 −28 35 32.3	11 Oct. 2019	00:49	1536	<2.5e-3	<2.2e-13	1527	>20.53
20 35 04.52 −05 47 35.3	04 Sep. 2019	12:23	1504	<3.6e-3	<3.2e-13	1485	>20.65

have performed some quick exploratory observations of three of the AO-SySt discovered in this paper with the *Swift* satellite (Gehrels et al. 2004), and for comparison of three of the identified radial pulsators considered as a control sample. The observations have been carried out in Target-of-Opportunity mode. This type of observations is generally limited to roughly 2000 seconds per object, so this can be considered as a quick and rather shallow survey of our target sample. The pointings were performed in two time slots: the first one in September-October 2019, and the second one in June 2020. The results are summarized in Table 8.

Our *Swift* observations were acquired with the on-board instruments X-Ray Telescope (hereafter XRT, Burrows et al. 2005) and UltraViolet-Optical Telescope (hereafter UVOT, Roming et al. 2005). The XRT allows covering the X–ray band between 0.3 and 10 keV band, whereas UVOT data were collected using the UV filter $UVM2$ (reference wavelength: 2246 Å; see Poole et al. 2008 and Breeveld et al. 2011 for details). On-source pointings were simultaneously performed with the two instruments and lasted between ∼500 and ∼2500 s.

All observations were reduced within the FTOOLS environment (Blackburn 1995). The XRT data analysis was performed using the XRTDAS standard pipeline package (XRTPIPELINE v. 0.13.4) in order to produce screened event files. All X–ray data were acquired in photon counting (PC) mode (Hill et al. 2004) adopting the standard grade filtering (0-12 for PC) according to the XRT nomenclature. For each source, scientific data were extracted from the images using an extraction radius of 47″ (20 pixels) centered at the optical coordinates of the source, while the corresponding background was evaluated in a source-free region of radius 94″ (40 pixels) within the same XRT acquisition. In all cases, no emission above a signal-to-noise threshold $S/N = 3$ was detected. The XRT count rate upper limits in the 0.3–10 keV range were then measured within the XSPEC package.

X–ray flux limits were determined using the WEBPIMMS online tool[3] by assuming a spectral model similar to the one used in Mukai et al. (2016) for SU Lyn, i.e. a thermal plasma emission with temperature $kT = 17$ keV absorbed by a column density $N_H = 2.9{\times}10^{22}$ cm^{-2}, which implies a count rate-to-flux conversion factor of ∼$8.8{\times}10^{-11}$ erg cm^{-2} s^{-1} cts^{-1}. We note that, with this model, the unabsorbed fluxes (in Table 8) in this same band are about 50% larger than the absorbed ones.

Count rates on Level 2 (i.e. calibrated and containing astrometric information) UVOT images at the position of the objects of our sample were measured through aperture photometry using 5″ apertures, whereas the corresponding background was evaluated for each image using a combination of several circular regions in source-free nearby areas. Magnitudes and upper limits were measured with the UVOTSOURCE task. The data were then calibrated using the UVOT photometric system described by Poole et al. (2008).

Of the three AO-SySt observed with *Swift*, two were found to be strong UV emitters, confirming their symbiotic nature. The third, GaSS 1-31 was not detected. There may be a clear reason for that, though. The *Swift* pointing was carried out on 14 June 2020. A few weeks later, on 5 July 2020, we observed the same star with the the Asiago 1.82m and the Echelle spectrograph. The Hα profile for that date is presented in Figure 7, and doesn't show the faintest trace of an emission. In addition, the equivalent width of the Hα absorption is same as for field stars of the same spectral type (and greater than for the other dates in Figure 7), indicating no partially filling from even very faint emission. In short, it looks like the emission from the accretion disk was 'switched-off' at the time of the *Swift* pointing, with consequent no detection. An eclipse behind the M-giant seems improbable in view of the limited variability of the epoch GALAH and Asiago radial velocities listed in Table 6 (and their similarity with the average velocity provided by Gaia DR2), precluding an high orbital inclination for GaSS 1-31. It rather seems a drastic reduction in the mass accretion rate was taking place at the time of *Swift* observations. This could have been caused by a reduction in the wind blown-off the M giant or passage at apo-astron in a highly eccentric orbit. The spectrum taken a hundred days later (that for 3 oct 2020 in Figure 7) shows that accretion has weakly resumed, with both a reduction in the equivalent width of Hα absorption (partially filled-in) as well as emission wings extending above the local continuum.

None of the three radial pulsators we tried with *Swift* was detected, in spite having been selected among those showing the strongest Hα and Hβ emission on GALAH spectra (far stronger than typically observed in AO-SySt). This

[3] `https://heasarc.gsfc.nasa.gov/cgi-bin/Tools/w3pimms/w3pimms.pl`

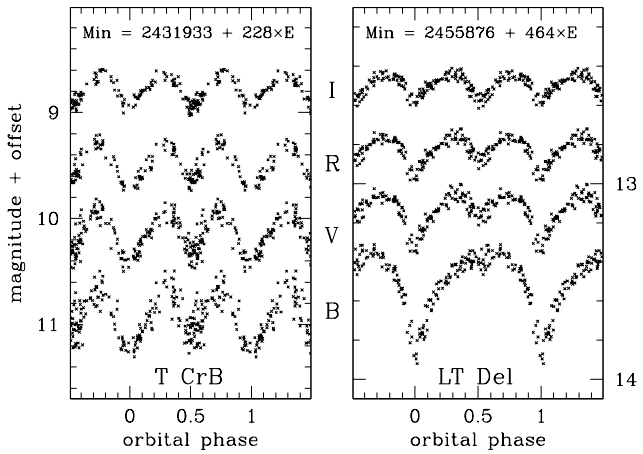

Figure 9. Examples of the modulation of the *BVRI* lightcurves induced by orbital motion in non-eclipsing symbiotic stars (see sect. 5.6). Note the increasing impact of flickering going toward bluer bands for the accreting-only T CrB, and its absence for the burning-type LT Del. The lightcurves are obtained from data extending over at least 10 consecutive orbital cycles. Adapted from Munari (2019).

supports the clear-cut role of satellite UV observations in segregating AO-SySt from radial pulsators of similar spectral appearance on optical spectra.

A few final words are in order to explain the non-detection of GaSS 1-11 and 1-12 in X-rays in our shallow observations. The upper limit to their flux is about 0.01× the flux recorded from SU Lyn during the *Swift* observations of Mukai et al. (2016). Those observations of SU Lyn were obtained during an exceptionally bright state of the accretion disk (cf. Figure 2 and the discussion at the end of sect. 2), while the flux at other times (when the Hα shown by SU Lyn is much weaker and more similar in appearance to that revealed by GALAH spectra for our sample of 33 AO-SySt) was just 1/10 of that (cf. Lopes the Oliveira et al. 2018). There are two other factors playing against GaSS 1-11 and 1-12. The most important is the distance. SU Lyn is just 0.65 kpc away, while the lower limit to the distance to GaSS 1-11 and 1-12 is 3.1 and 2.4 kpc, respectively (cf. Table 5), corresponding to dilution factors of ≥23 and ≥14, respectively. In addition, SU Lyn is seen face-on, while the unknown orbital inclination of GaSS 1-11 and 1-12 introduces a reduction in flux proportional to $\cos i$ and in addition a further reduction for limb-darkening reasons. Considering all factors together, there is no wonder that GaSS 1-11 and 1-12 felt below the X–ray detection threshold of snapshot ToO with *Swift*.

5.6 Orbital-like periodicities

Aside from the obvious effect of eclipses for systems seen at high inclination, the orbital motion can model also the lightcurve of symbiotic stars seen at an intermediate inclination. The basic appearance of such a lightcurve is shown in Figure 9 (adapted from the review of Munari 2019).

We have already mentioned that the recurrent nova T CrB is an AO-SySt. Its M3III giant fills the Roche lobe, causing an ellipsoidal deformation of the surface, that along an orbital period presents to observers twice the larger projected area (the two maxima in the lightcurve) and twice the smaller one (the two minima). The reason for the change in brightness is primarely geometric, so its shape is similar at all wavelengths as the left panel of Figure 9 shows. In that figure, the presence of flickering superimposed to the regular orbital motion is quite obvious, in the form of a scatter of points of an increasing amplitude moving from redder to bluer bands (cf. sect 5.4 above). A search for periodicity on such a lightcurve would return *half* the value of the true period: 114 days instead of 228. It is the spectroscopic orbit that would solve the uncertainty in favor of 228 days.

The M4III giant in LT Del, the other symbiotic star in Figure 9, equally fills its Roche lobe. At the reddest wavelengths, its orbitally modulated lightcurves look identical to that of T CrB. It is however moving toward bluer bands where differences in the primary and secondary minima begin to emerge: in *B* band (and evidently even more so in *U*) primary minima are much deeper, and it is not necessary to invoke assistance from the spectroscopic orbit to distinguish among the true 464 day period and half this value. The deeper primary minima trace the transit at inferior conjunction of the M giant and thus the partial obscuration of its side facing the companion. If the companion is hot and bright, it causes an irradiation of the facing side of the M giant, thus heating the photosphere and partially ionizing the atmosphere above it, with the consequence to make the system brighter when this irradiated side is in full view (Kenyon 1986). In the case of LT Del the irradiation is particularly robust given the fact that its WD is experiencing stable nuclear burning at the surface.

We have searched the ASAS-SN photometric data for the 33 candidate AO-SySt looking for a type of lightcurve modulation that could be orbitally induced along the lines just outlined for T CrB and LT Del in Figure 9. We found a suitable shape for 12 of them, and they are presented in Figure 10 and the periods listed in Table 5. Their length is rather typical for symbiotic stars, the majority of known cases going from 7 months to 2.5 years (Mikołajewska 2003).

In two cases, GaSS 1-27 and GaSS 1-28, a slight difference in the depth of minima seems enough to resolve the ambiguity between P and 2×P. Given the limited time span of ASAS-SN coverage, such a difference could also result from other causes for photometric variability, and needs confirmation over more orbital cycles. Even more so for a possible third case for unequal minima, that of GaSS 1-33, and its sparsely covered lightcurve (cf Figure 10). A borderline case is that of GaSS 1-8, with just a hint of a secondary minimum around phase 0.5 which could be spurious.

The remaining objects in Figure 10 show equal-depth minima, so the actual orbital period could be twice the value listed in Table 5 and on the ephemerises in their respective panels of Figure 10. To help resolve the controversy, we have started a *BVRI* monitoring of them all, but the fruits of that labour will be collected only in a few years time, when at least a few orbital cycles will be covered.

5.7 Lithium

Wallerstein et al. (2008), in their chemical analysis of high resolution spectra of M giants in symbiotic stars, found that the accreting-only systems T CrB and RS Oph show a large over-abundance of ^{7}Li in their spectra. None of the other symbiotic stars in their large sample showed ^{7}Li enhance-

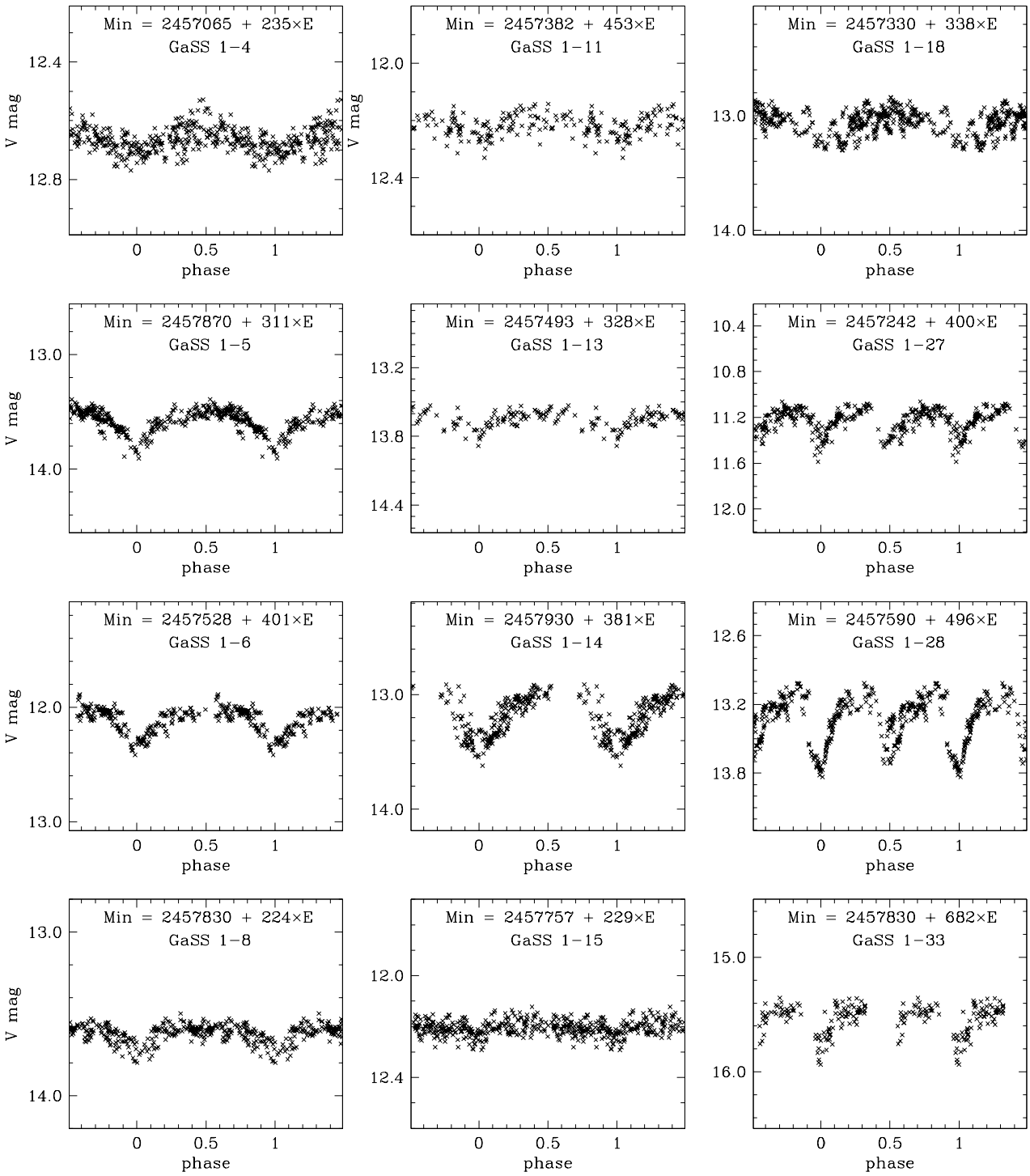

Figure 10. Phased light-curves (see ephemeris at the top of each panel) for the twelve AO-SySt marked in Table 5 as showing a modulation reminiscent of orbital motion.

ment and none was known to have undergone nova outbursts. The apparent link between ^{7}Li and nova outbursts was further reinforced when the symbiotic star V407 Cyg erupted in 2010. ^{7}Li over-abundance was discovered earlier in V407 Cyg by Tatarnikova et al. (2003) at a time when the object was simply known as a Mira variable with a possible companion, and therefore attributed to indigenous production via the Cameron & Fowler (1971) mechanism activated in the asymptotic giant branch star. The over-abundance of ^{7}Li in T CrB has been recently revised upward to A(Li) = 2.4±0.1 by Woodward et al. (2020).

The production of ^{7}Li during nova eruptions has been predicted theoretically (e.g. José & Hernanz 1998, Rukeya et al. 2017, Starrfield et al. 2020) and confirmed observationally (e.g. Tajitsu et al. et al. 2015, Izzo et al. 2015, Molaro et al. 2016). Up to ~1×10^{-5} of the whole mass of the ejecta can

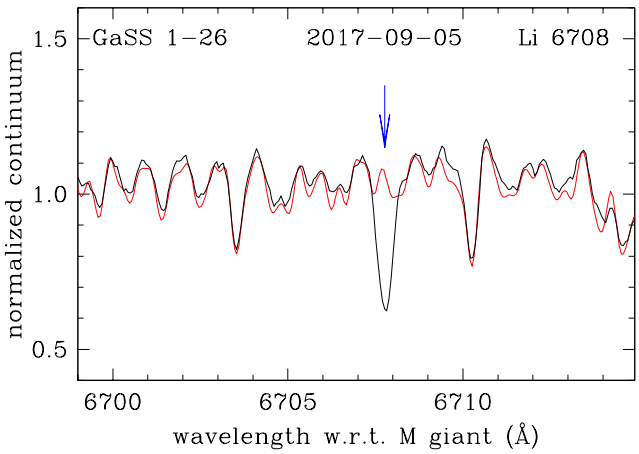

Figure 11. The GALAH spectrum of GaSS 1-26 (black) around the position of LiI 6707.8 Å compared with that (red) of the template for the same f-ratio bin. The overabundance of LiI is quite obvious.

be in the form of ^{7}Li, actually ^{7}Be that will decay into ^{7}Li (Starrfield et al. 2020). The large amounts produced during outbursts (especially those occourring on white dwarfs of the Carbon-Oxigen type), suggests that novae could be the main producer of ^{7}Li in the Milky Way (Molaro et al. 2020).

It is tempting to attribute the over-abundance of ^{7}Li observed in the AO-SySt T CrB, RS Oph and V407 Cyg to pollution of the cool giant by the ejecta of the nova outbursts experienced by the WD companion. Their eruptions occour at a high frequency (eight have been observed in historic times for RS Oph) such that they replenish the surface of the cool giant with ^{7}Li much faster than convection can dilute ^{7}Li into the interior of the star. In alternative, ^{7}Li could instead come from the interior of the cool giant, and conditions leading to an efficient transport of ^{7}Li to the surface could also lead more probably to nova outbursts as a consequence of a higher mass loss rate and/or an enrichment in CNO nuclei.

We have searched for ^{7}Li overabundance in our 33 AO-SySt by comparing with the template spectrum for their f-bin, and found a clear case of enhancement in GaSS 1-26, as shown in Figure 10. The object is completely anonymous (no matching entry in SIMBAD, VSX and similar catalogs) and its optical variability is inconspicuous (cf Figure A7 in the Appendix). It lies outside the region of the sky so far covered by digitization of historical Harvard photographic plates (E. Los, private communication), so a visual inspection of the many plates covering GaSS 1-26 position in search for a nova outburst that went unnoticed in a distant past needs to wait for the end of the current pandemic and lift of consequent restrictions. It is clearly an object worth a dedicated effort to obtain a wide range of follow-up observations.

In favor of a possible pollution scenario for the ^{7}Li in GaSS 1-26 is the fact that indigenous ^{7}Li production via the the Cameron & Fowler (1971) mechanism is expected to occour during hot-bottom burning conditions (HBB), when the outer part of the burning H-shell is included in the envelope convection. A key aspect of HBB is the existence of a lower mass limit for it to occour, which depends on metallicity (Herwig 205). The minimum initial mass for HBB is $M_{ini} \geq 5$ $M_\odot$ at solar metallicity (Forestini & Charbonnel 1997), which can decrease down to 3 $M_\odot$ for *very* metal-poor stars (Siess, Livio and Lattanzio 2002). The latter is obviously not the case given the otherwise normal spectrum displayed by GaSS 1-26. The faintness and negligible reddening place GaSS 1-26 at a great distance from us, estimated to 6.0 kpc in Table 5 (this is actually a lower limit should the luminosity class of the M giant be higher that the adopted class III). At a galactic latitude $-10\overset{\circ}{.}6$, it means an height over the galactic plane of $z \geq 1.1$ kpc. It would be rather atypical to find a young and massive $M_{ini} \geq 5$ $M_\odot$ star that distant from the galactic plane.

6 CONCLUSIONS AND FUTURE PROSPECTS

We present the discovery and characterisation of 33 bona-fide candidates of the *accreting-only* type of symbiotic stars (AO-SySt). So far, this class of binary systems has evaded a thorough scientific scrutiny, otherwise received by its counterpart, the *burning-type* class of symbiotic stars (NB-SySt). Both describe the same underlying configuration, a binary system composed of an RGB star and a compact companion, however, they are distinguished by the physical processes under way inside the system and the consequent observational implications, favouring the study of NB-SySt. Because AO-SySt are believed to be much more abundant in the Galaxy than NB-SySt, while the ratio of known (investigated) objects is just the reverse, it is important to uncover this hidden population of interacting binary stars in order to asses the viability of symbiotic stars as progenitors of type Ia supernovae, their impact on the pollution of the ISM, and to better understand the cycle of exchange between the *accreting-only* and *burning-type* phase.

To this end, we have investigated a large sample of 600 255 stars from the GALAH spectroscopic all-sky survey, which, given its unbiased observational strategy, promises to enable the envisaged statistical analysis, while supported by a suite of follow-up observations, provides a rich source of information on individual symbiotic stars. The first 33 candidates presented in this paper were selected using relatively conservative criteria: parallax and colour cut, strength of molecular (TiO) absorption bands, prominence of Hα emission line, rejection based on the presence of various observational and reduction artefacts. Furthermore, the photometric light curves were checked to filter out radial pulsators, and great care was taken to reinforce our diagnostics for the symbiotic nature of program stars, building on the knowledge provided by the prototype AO-SySt SU Lyn and by conducting follow-up ground and space based observations examining the near-UV excess, RV and emission line variability, optical flickering, and X–ray/UV luminosities.

Future studies will extend the analysis presented in this work in diverse directions, including:

- weaker emission features in spectra will be considered, as we currently only accept Hα profiles which, after subtraction of the template spectrum, reach higher than 0.5 above the adjacent continuum
- other spectral diagnostic features will be established to identify AO-SySt despite a possible absence of emission lines, for example a peculiar chemical signature in the spectrum of a giant star that was polluted by eruptions from the

compact companion and thus by nuclearly processed material

- earlier spectral types of the primary stars will be investigated, also to account for the more metal-poor systems which do not achieve the same large radius and low surface temperatures as M giants
- automatic and manual inspection of legacy observations is being carried out, such as digging through diverse photometric archives and historical plates stacks in order to find e.g. past active phases or nova outbursts
- existing and future high-energy instruments/surveys (e.g. SWIFT, *e*-ROSITA) can be exploited for follow-up observations or cross-matching of catalogued detections
- combining the chemical abundances and galactic orbits with the aid of the next Gaia releases will provide the means to confirm/reject the belief of symbiotic stars being an old population, primarily belonging to the bulge, thick disk, and halo. This view is built from the infrared characteristics of their cool giants, but it is heavily biased by how (and where in the Galaxy) the classical symbiotic stars were discovered by objective prism surveys of half a century ago. Determining the parent stellar population of symbiotic stars has profund implication considering that Ia supernovae are the only type known to erupt in elliptical galaxies, whose stellar population resemble the Bulge of our Galaxy.

The proposed future work will greatly expand the number of characterised AO-SySt and thus provide the community with large enough samples for a statistical study of the population of symbiotic stars as a whole. In the meantime, we encourage the readers to further investigate the 33 candidates presented here and help confirm their symbiotic nature with follow-up observations.

ACKNOWLEDGEMENTS

This research has made use of the ASI Science Data Center Multimission Archive; it also used the NASA Astrophysics Data System Abstract Service, which is operated by the Jet Propulsion Laboratory, California Institute of Technology, under contract with the National Aeronautics and Space Administration. This research has also made extensive use of the SIMBAD and VIZIER databases operated at CDS, Strasbourg, France. We thank Dr. Jamie Kennea and the *Swift* team for the quick approval and the rapid acquisition of the observations we requested. NM acknowledges financial support through ASI-INAF agreement 2017-14-H.0. We would also like to thank S. Dallaporta, A. Vagnozzi and G.L. Righetti (ANS Collaboration) for useful test observations.

REFERENCES

Akras S., Guzman-Ramirez L., Leal-Ferreira M. L., Ramos-Larios G., 2019, ApJS, 240, 21
Allen D. A., 1984, PASAu, 5, 369
Barden S. C., et al., 2010, SPIE, 7735, 773509, SPIE.77351
Belczyński K., Mikołajewska J., Munari U., Ivison R. J., Friedjung M., 2000, A&AS, 146, 407
Blackburn J. K., 1995, ASPC, 77, 367, ASPC...77
Bragaglia A., Duerbeck H. W., Munari U., Zwitter T., 1995, A&A, 297, 759
Breeveld A. A., Landsman W., Holland S. T., Roming P., Kuin N. P. M., Page M. J., 2011, AIPC, 1358, 373, AIPC.1358
Burrows D. N., et al., 2005, SSRv, 120, 165
Cameron A. G. W., Fowler W. A., 1971, ApJ, 164, 111
Cheung C. C., Donato D., Wallace E., Corbet R., Dubus G., Sokolovsky K., Takahashi H., 2010, ATel, 2487, 1
de Laverny P., Recio-Blanco A., Worley C. C., Plez B., 2012, A&A, 544, A1261
De Silva G. M., et al., 2015, MNRAS, 449, 2604
Dobrzycka D., Kenyon S. J., Milone A. A. E., 1996, AJ, 111, 414
Evans P. A., Page K. L., Osborne J. P., Beardmore A. P., Willingale R., Burrows D. N., Kennea J. A., et al., 2019, yCat, IX/58
Fluks M. A., Plez B., The P. S., de Winter D., Westerlund B. E., Steenman H. C., 1994, A&AS, 105, 311
Forestini M., Charbonnel C., 1997, A&AS, 123, 241
Freeman K., Bland-Hawthorn J., 2002, ARA&A, 40, 4871
Fujimoto M. Y., 1982, ApJ, 257, 767
Gaia Collaboration, et al., 2018, A&A, 616, A11
Gehrels N., et al., 2004, ApJ, 611, 1005
Izzo L., Della Valle M., Mason E., Matteucci F., Romano D., Pasquini L., Vanzi L., et al., 2015, ApJL, 808, L14.
Hellier C., 2001, Cataclysmic Variable Stars, Springer
Henden A. A., Templeton M., Terrell D., Smith T. C., Levine S., Welch D., 2016, yCat, II/336
Henize K. G., 1976, ApJS, 30, 491.
Herwig F., 2005, ARA&A, 43, 435.
Hill J. E., et al., 2004, SPIE, 5165, 217, SPIE.5165
Hinkle K. H., Fekel F. C., Joyce R. R., Wood P., 2013, ApJ, 770, 28
Hoffmeister C., Richter G., Wenzel W., 1985, Variable Stars, Springer-Verlag, Berlin
Howell S. B., et al., 2014, PASP, 126, 3981
José J., Hernanz M., 1998, ApJ, 494, 680.
Joy A. H., 1926, ApJ, 63, 281
Karovska M., 2006, ESASP, 604, 183, ESASP.604
Kenyon S. J., 1986, The Symbiotic Stars, Cambridge Univ. Press
Kenyon S. J., Fernandez-Castro T., 1987, AJ, 93, 938
Kochanek C. S., et al., 2017, PASP, 129, 104502
Koornneef J., 1983, A&A, 500, 247
Kos J., et al., 2017, MNRAS, 464, 12591
Kuranov, A.G., & Postnov, K.A. 2015, Astron. Lett., 41, 114
Landolt A. U., 1992, AJ, 104, 340.
Lee T. A., 1970, ApJ, 162, 217
Lopes de Oliveira, R., Sokoloski, J.L., Luna, G.J.M., Mukai, K., & Nelson, T. 2018, ApJ, 864, 46
Martell S. L., et al., 2017, MNRAS, 465, 32031
Masetti, N., Landi, R., Pretorius, M. L., et al. 2007, A&A, 470, 331
Massey P., 2002, ApJS, 141, 81.
Merrill P. W., 1940, The Spectra of Long-Period Variable Stars, Univ. Chicago Press
Merrill P. W., Burwell C. G., 1950, ApJ, 112, 72.
Mikołajewska J., 2003, ASPC, 303, 9
Mikolajewski M., Mikolajewska J., Tomov T., Kulesza B., Szczerba R., Wikierski B., 1990, AcA, 40, 129
Molaro P., Izzo L., Mason E., Bonifacio P., Della Valle M., 2016, MNRAS, 463, L117.
Molaro P., Izzo L., Bonifacio P., Hernanz M., Selvelli P., della Valle M., 2020, MNRAS, 492, 4975.
Morgan W. W., Keenan P. C., Kellman E., 1943, *An Atlas of Stellar Spectra*, Chicago Univ. Press
Morgan W. W., Keenan P. C., 1973, ARA&A, 11, 29
Mukai K., et al., 2016, MNRAS, 461, L1
Munari, U., in *The Impact of Binary Stars on Stellar Evolution*, G. Beccari and H.M.J. Boffin eds., 2019, Cambridge Univ. Press,p. 77 (arXiv:190901389)
Munari U., Moretti S., 2012, BaltA, 21, 22.

Munari U., Renzini A., 1992, ApJL, 397, L87
Munari U., Margoni R., Stagni R., 1990, MNRAS, 242, 653
Munari U., Dallaporta S., Cherini G., 2016, NewA, 47, 7
Pearse R. W. B., Gaydon A. G., 1976, The Identification of Molecular Spectra, 4th ed., Chapman and Hall, London
Poole T. S., et al., 2008, MNRAS, 383, 627
Ricker G. R., et al., 2015, JATIS, 1, 0140031
Roming P. W. A., et al., 2005, SSRv, 120, 95
Rukeya R., Lü G., Wang Z., Zhu C., 2017, PASP, 129, 074201.
Sanduleak N., Stephenson C. B., 1973, ApJ, 185, 899.
Schlafly E. F., Finkbeiner D. P., 2011, ApJ, 737, 103
Siess L., Livio M., Lattanzio J., 2002, ApJ, 570, 329
Shappee B. J., et al., 2014, ApJ, 788, 48
Sharma S., et al., 2018, MNRAS, 473, 20041
Sheinis A., et al., 2015, JATIS, 1, 0350021
Skopal A., Shugarov S. Y., Masetti N., Marchesini E., Komžík R. M., Kundra E., et al., 2020, A&A, 636, A77.
Slovak M. H., Africano J., 1978, MNRAS, 185, 591
Skrutskie M. F., et al., 2006, AJ, 131, 11631
Sokoloski J. L., Bildsten L., Ho W. C. G., 2001, MNRAS, 326, 553
Sowell J. R., Trippe M., Caballero-Nieves S. M., Houk N., 2007, AJ, 134, 1089.
Starrfield, S., Iliadis, C., Hix, W. R. 2008, in Classical Novae 2nd ed., M. F. Bode and A. Evans eds., CAS 43, Cambridge Univ. Press.
Starrfield S., Bose M., Iliadis C., Hix W. R., Woodward C. E., Wagner R. M., 2020, ApJ, 895, 70.
Sterken C., Jaschek C., 2005, eds. Light Curves of Variable Stars, Cambridge Univ. Press
Tajitsu A., Sadakane K., Naito H., Arai A., Aoki W., 2015, Natur, 518, 381.
Tatarnikova A. A., Marrese P. M., Munari U., Tomov T., Whitelock P. A., Yudin B. F., 2003, MNRAS, 344, 1233.
Tomov T., Kolev D., Ivanov M., Antov A., Jones A., Mikolajewski M., Lepardo A., et al., 1996, A&AS, 116, 1
Turnshek D. E., Turnshek D. A., Craine E. R., Boeshaar, P. C., 1985, An Atlas of Digital Spectra of Cool Stars, Western Research Co., Tucson
Wallerstein G., Harrison T., Munari U., Vanture A., 2008, PASP, 120, 492.
Warner B., 1995, Cataclysmic Variable Stars, CAS 28, Cambridge Univ. Press
Wittenmyer R. A., et al., 2018, AJ, 155, 841
Woodward C. E., Pavlenko Y. V., Evans A., Wagner R. M., IIyin I., Strassmeier K. G., Starrfield S., et al., 2020, AJ, 159, 231.
Yamashita Y., Nariai K., 1977, An Atlas of Representative Stellar Spectra, Univ. of Tokyo Press
Zamanov R., Boeva S., Latev G., Stoyanov K., Bode M. F., Antov A., Bachev R., 2011, IBVS, 5995, 1

Table 1. Log of low-resolution spectroscopic observations obtained with the Asiago 1.22m + B&C + 300 ln/mm (3300-8000 Å, 2.31 Å/pix) in search for the near-UV upturn. The exposure time is in seconds.

SySt	UT middle		expt
GaSS 1-7	2020-06-18	20:40	120
GaSS 1-7	2020-06-27	20:32	960
GaSS 1-9	2019-08-09	19:59	480
GaSS 1-9	2019-08-16	19:43	480
GaSS 1-9	2019-09-01	19:48	1200
GaSS 1-9	2020-06-27	22:31	960
GaSS 1-9	2020-08-25	19:18	480
GaSS 1-12	2019-08-16	20:27	720
GaSS 1-12	2019-08-19	20:54	960
GaSS 1-12	2019-09-01	19:27	1200
GaSS 1-12	2020-08-25	20:11	480
GaSS 1-13	2020-08-25	21:37	480
GaSS 1-13	2020-10-13	18:05	1800
GaSS 1-14	2019-08-30	18:59	480
GaSS 1-14	2019-09-01	20:18	960
GaSS 1-14	2019-12-06	17:24	1200
GaSS 1-15	2020-09-02	21:58	960
GaSS 1-15	2020-10-13	19:49	1800
GaSS 1-21	2020-06-19	21:24	720
GaSS 1-21	2020-06-27	21:54	1200
GaSS 1-23	2019-08-16	19:57	1200
GaSS 1-23	2019-08-19	19:41	960
GaSS 1-23	2019-09-01	19:58	1200
GaSS 1-23	2020-08-25	19:37	480
GaSS 1-25	2020-08-25	19:27	480
GaSS 1-28	2019-09-03	19:44	1200
GaSS 1-31	2020-08-25	20:20	480
GaSS 1-31	2020-10-13	17:30	1800
GaSS 1-33	2020-08-27	22:18	1440
GaSS 1-33	2020-10-13	20:28	3600

This paper has been typeset from a TEX/LATEX file prepared by the author.

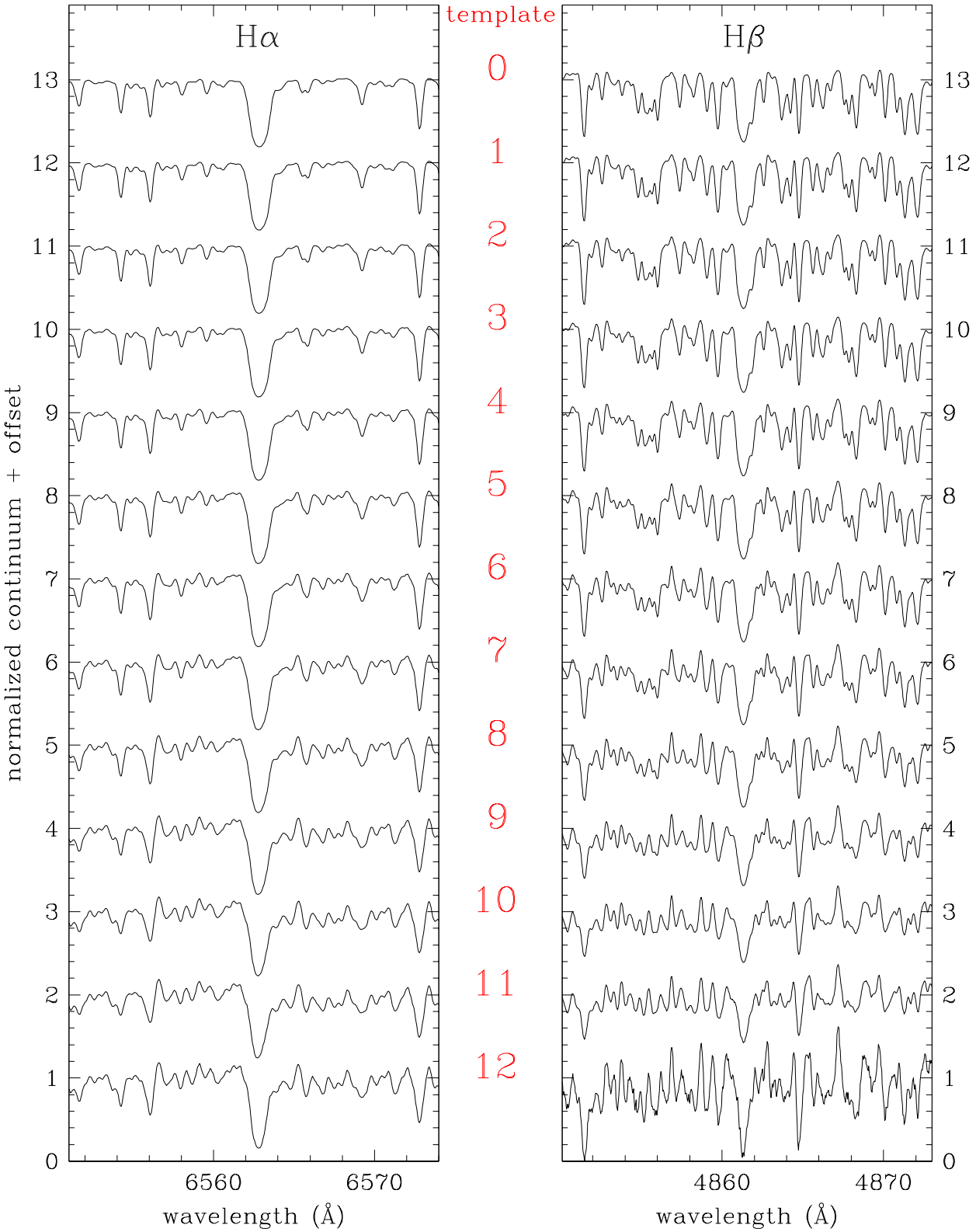

Figure 1. Sequence of templates listed in Table 4.

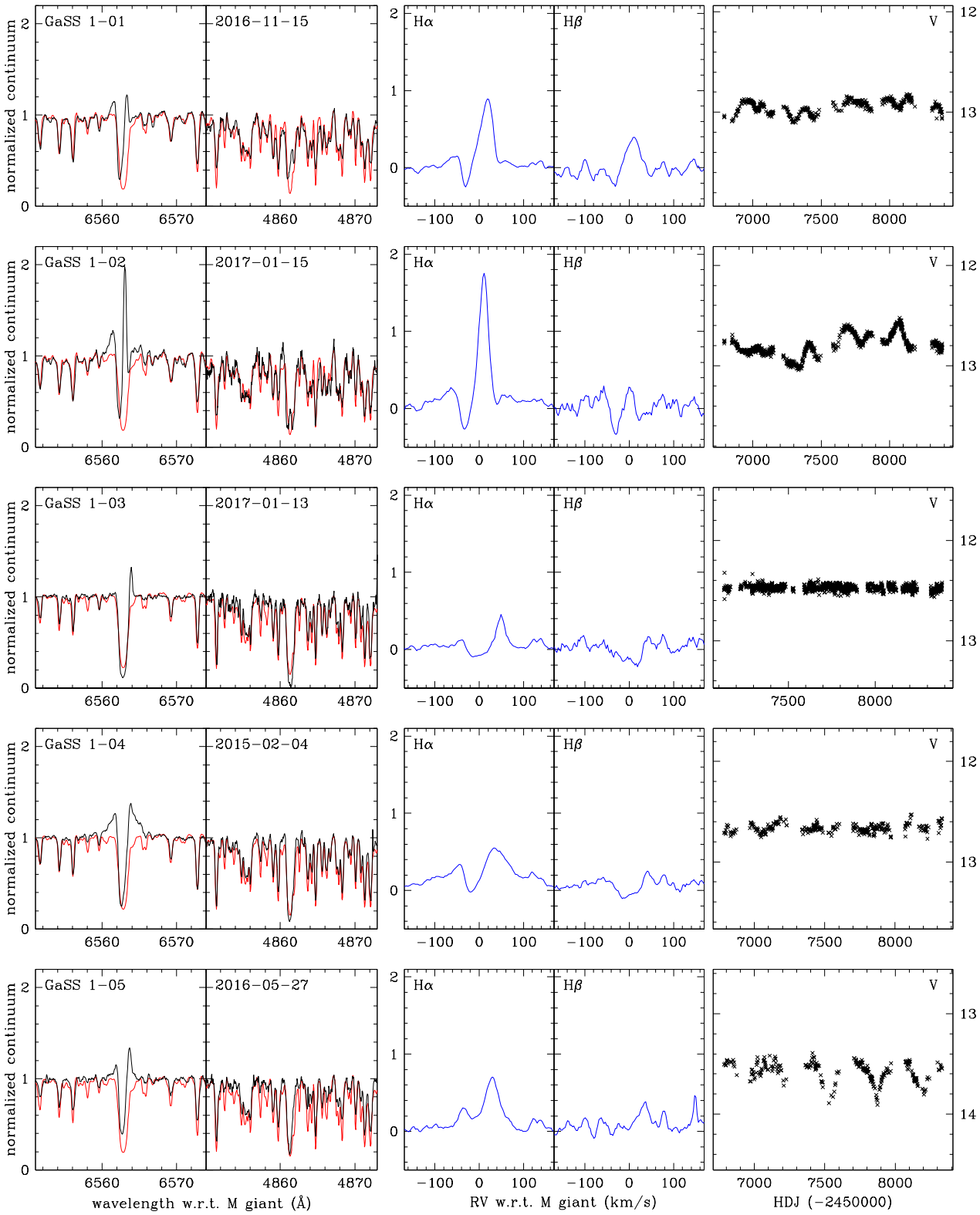

Figure 2. *Left-most panels*: Hα and Hβ profiles (in black) compared to respective templates (in red) for program stars GaSS 1-1 to GaSS 1-5. *Center panels*: the result of subtracting the template from the object spectrum. *Right-most panel*: *V*-filter lightcurve from ASAS-SN sky patrol data.

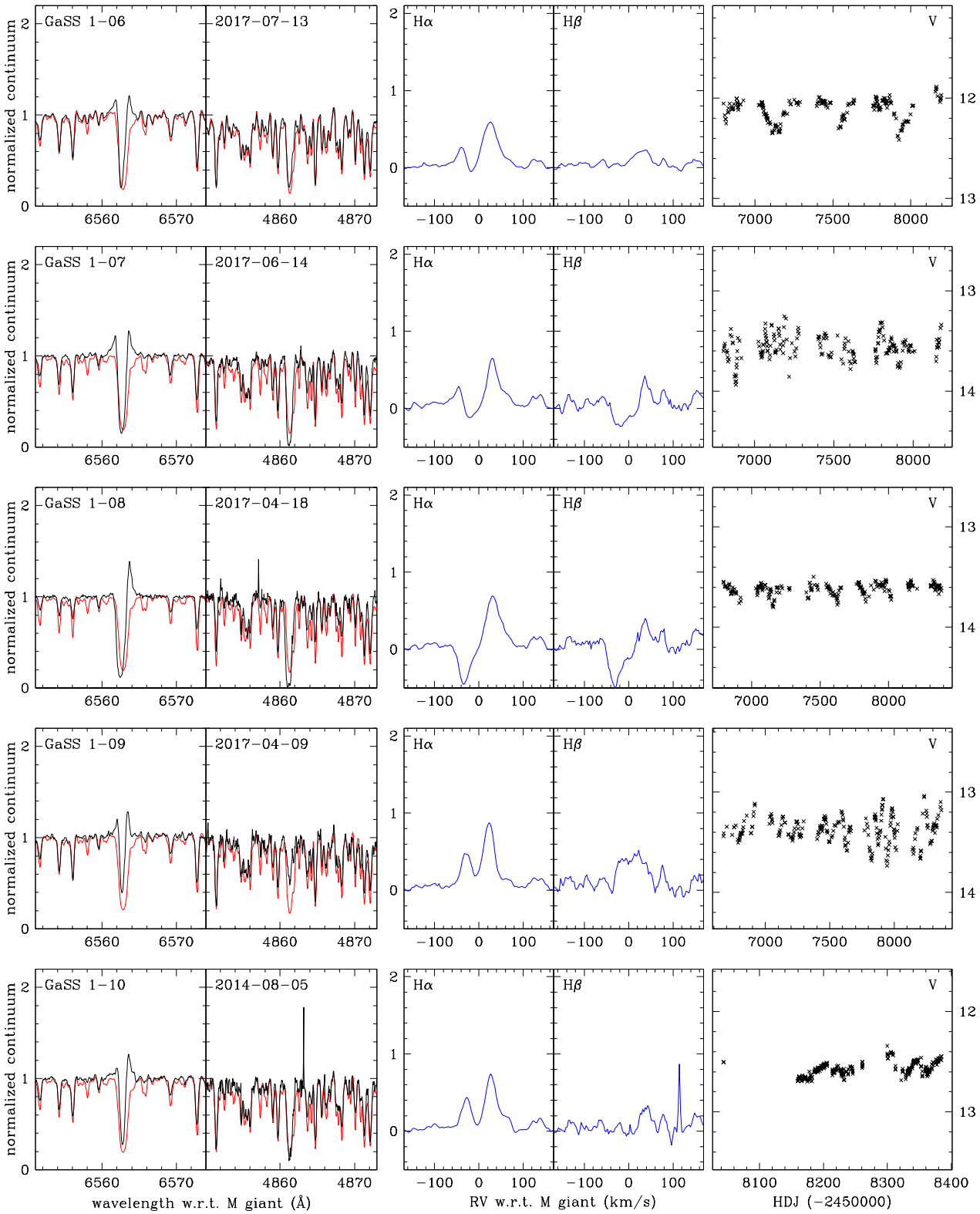

Figure 3. Similar to Figure A2 for program stars GaSS 1-1 to GaSS 6-10.

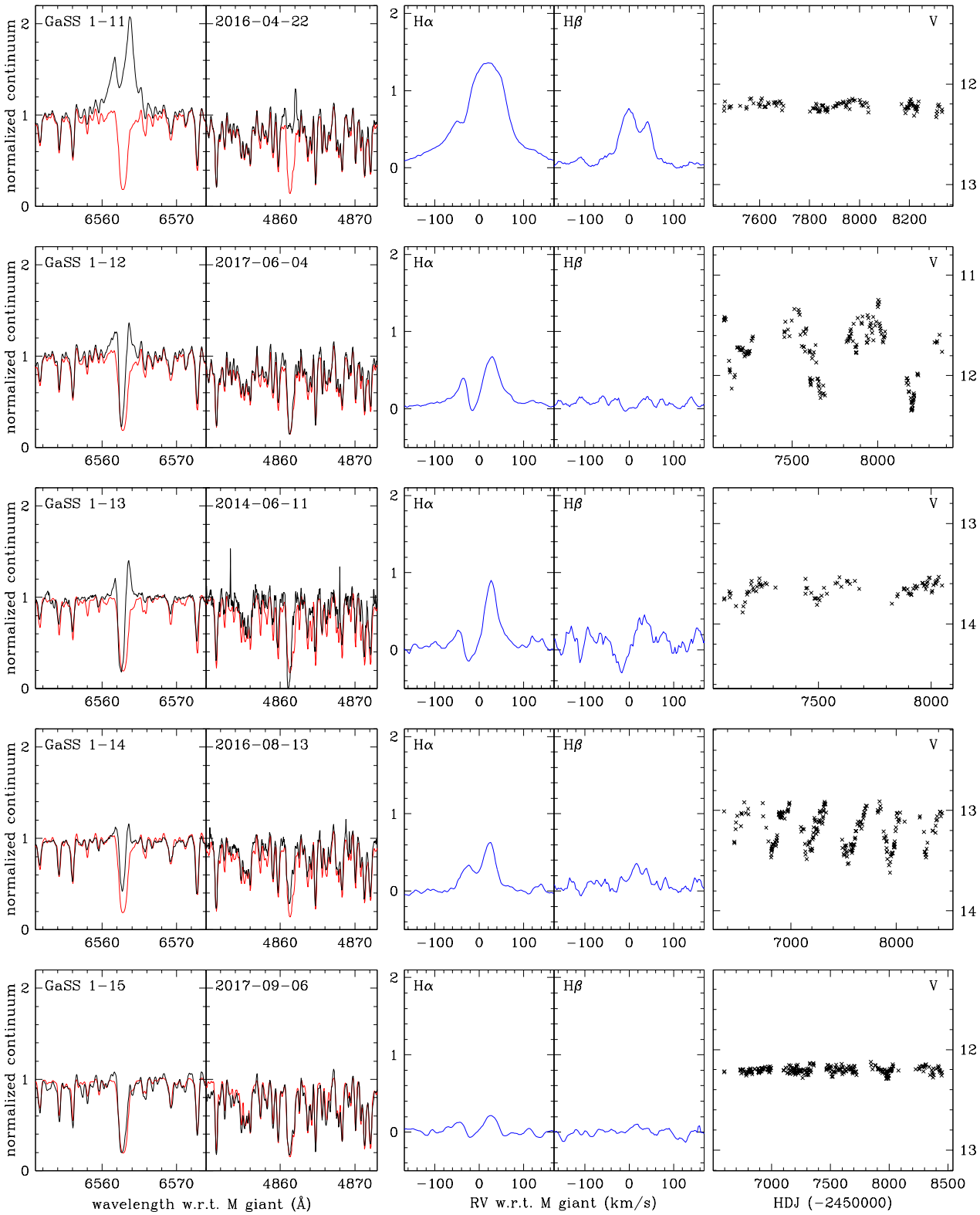

Figure 4. Similar to Figure A2 for program stars GaSS 1-1 to GaSS 11-16.

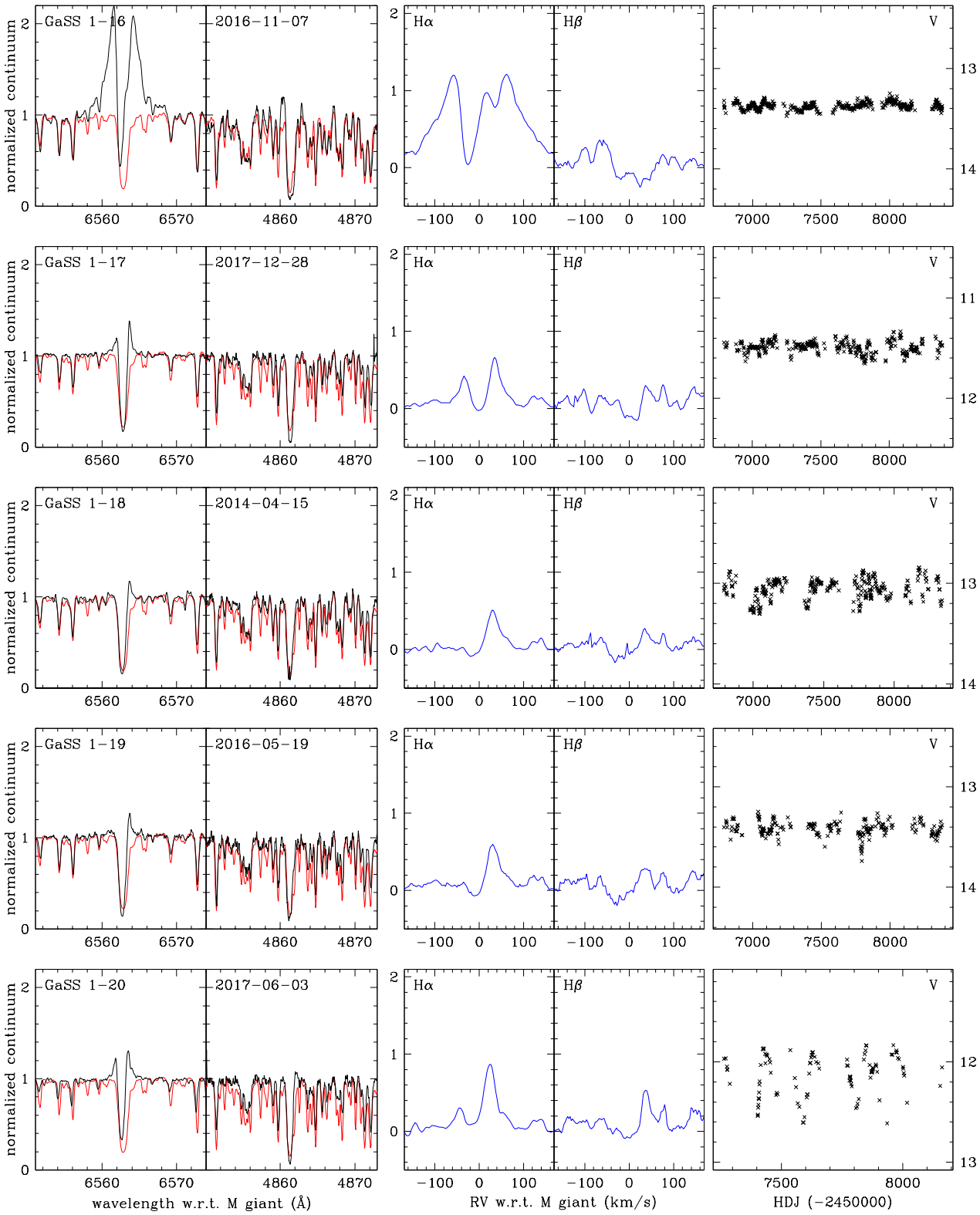

Figure 5. Similar to Figure A2 for program stars GaSS 1-1 to GaSS 17-20.

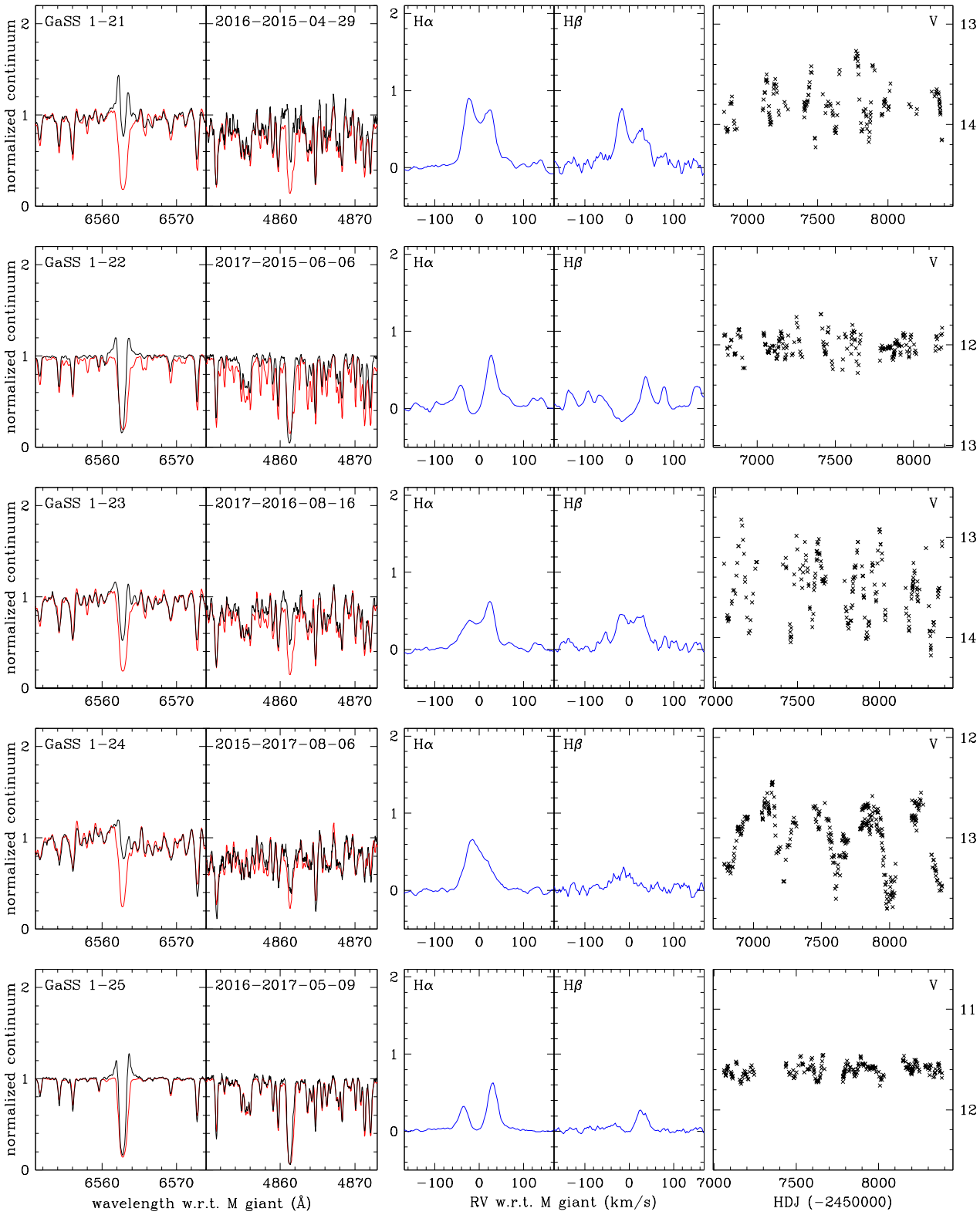

Figure 6. Similar to Figure A2 for program stars GaSS 1-1 to GaSS 21-25.

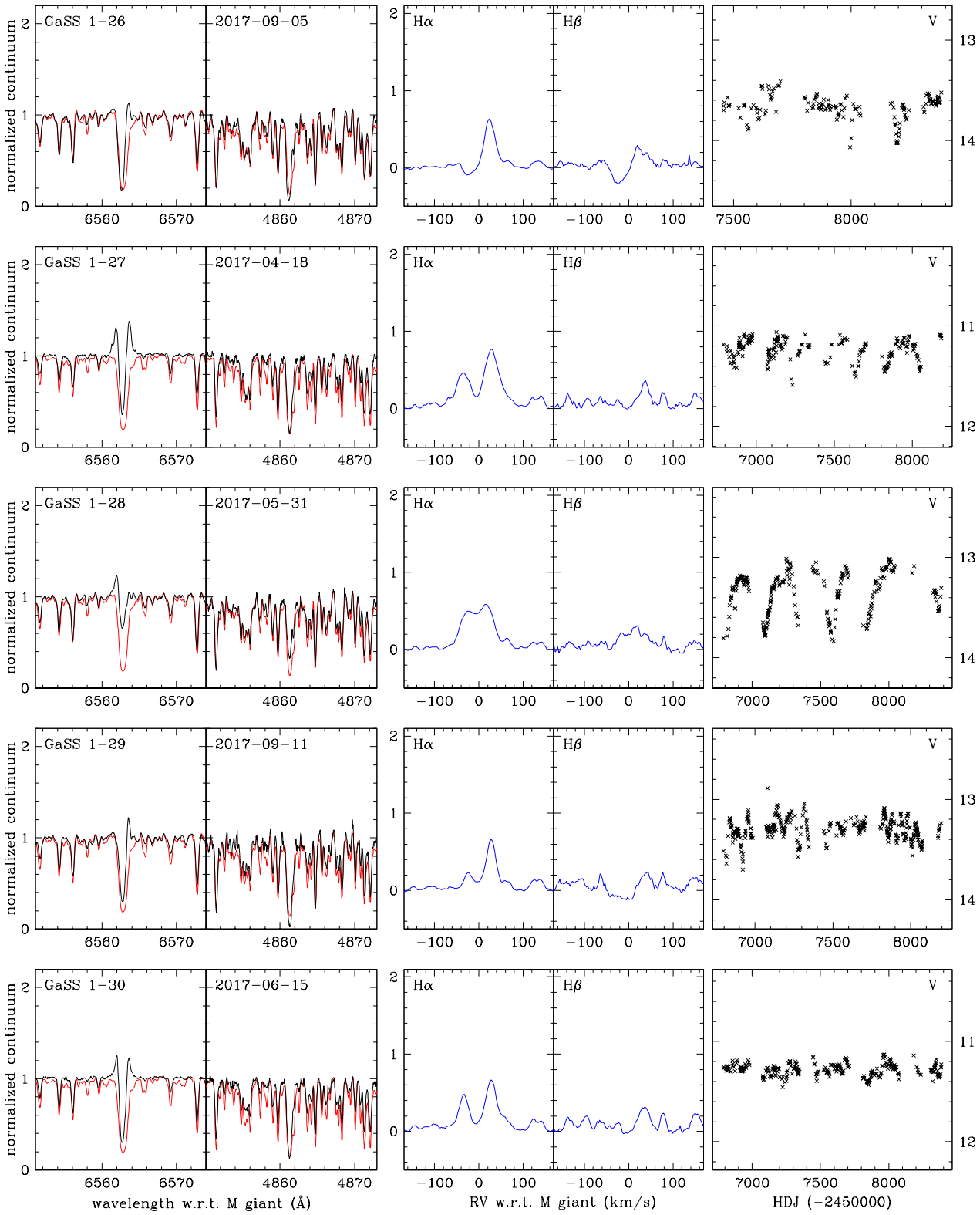

Figure 7. Similar to Figure A2 for program stars GaSS 1-1 to GaSS 26-30.

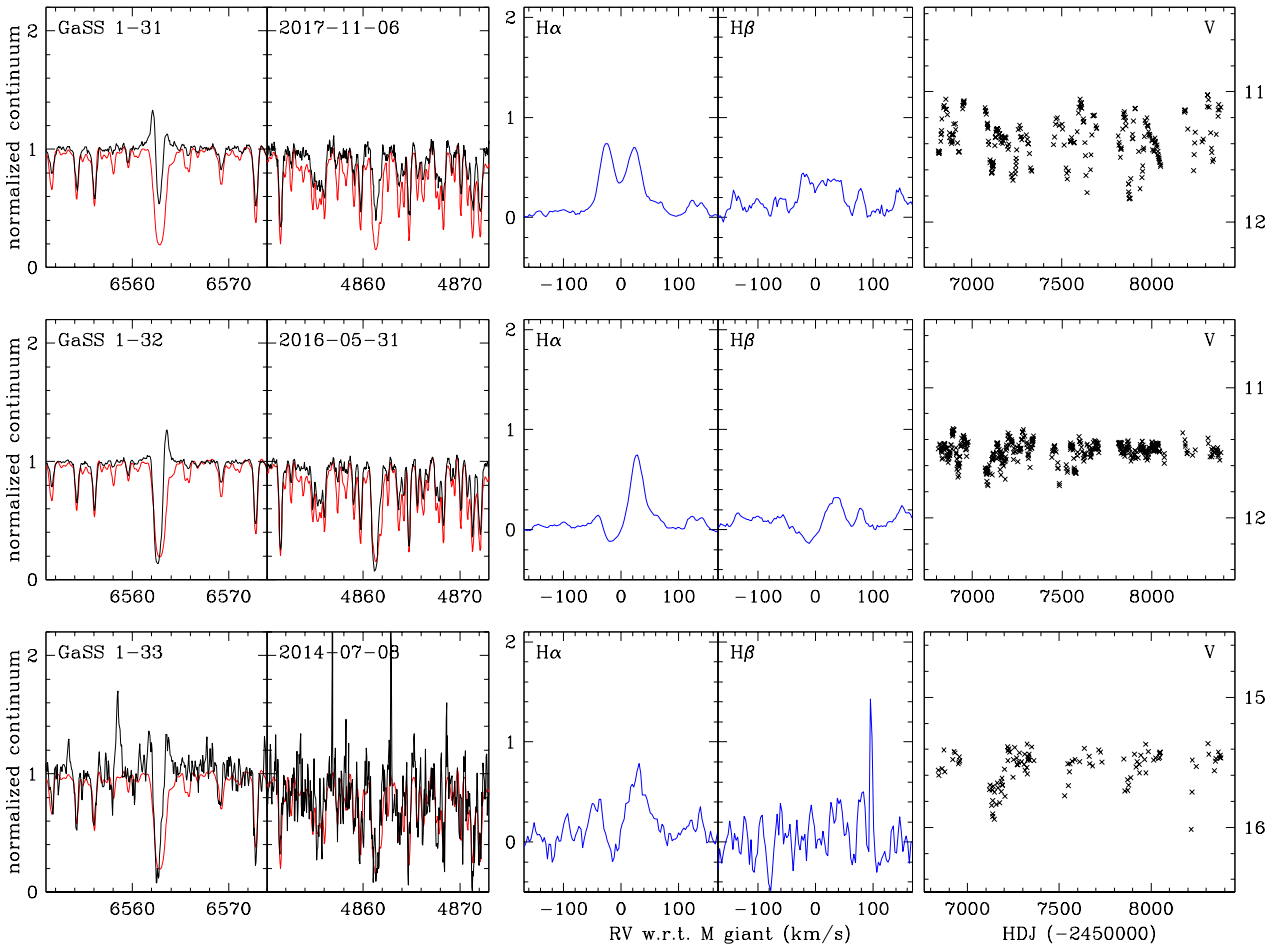

Figure 8. Similar to Figure A2 for program stars GaSS 1-1 to GaSS 31-33.